Journal of Intelligent Manufacturing
https://doi.org/10.1007/s10845-024-02558-1

A cyber-physical architecture to monitor human-centric reconfigurable manufacturing systems

Andrea Sbaragli[1] · Poorya Yazdi Ghafoorpoor[2] · Sebastian Thiede[2] · Francesco Pilati[1]

Received: 12 March 2024 / Accepted: 23 December 2024

Abstract

Reconfigurable manufacturing systems represent the most adequate production paradigm due to their ability to meet mass customized needs while ensuring cost-effective flexibilities and performances. However, digital solutions are required to manage these dynamic environments over working shifts and processes' reconfiguration. In this scenario, this work proposes a layout and task-insensitive cyber-physical architecture to monitor human-centric reconfigurable manufacturing systems. Workers' motion patterns and industrial resources' positions are acquired through a radio-frequency-based real-time locating system. These data streams are fed into a machine-learning cyber layer to segment operators' activities during production cycles into two steps. The first computational stream assigns workers' motion patterns to industrial resources regardless of the system configuration. The following step distinguishes workers' operations into value-added and non-value-added. These outputs are stored in a decision support system where customized callback functions develop key performing indicators to monitor the performance of such reconfigurable human-centric environments. The validity of the cyber-physical architecture is demonstrated in an industrial-related pilot environment, involving 40 workers and 8 production set-ups.

Keywords Reconfigurable manufacturing systems · Cyber-physical architecture · Machine learning · Real-time locating systems · Human-centric

Introduction

Over recent years, manufacturing companies have been facing several disruptions to their in-plant functioning and thus performances. Among the others, mass customization of goods is pushing manufacturing environments to achieve a wider product portfolio (Zhang et al., 2019). Consequently, production batch sizes are reduced to meet final customers' requests (Suzić et al., 2018). This notable market-driven trend requires industrial environments to offer unprecedented production flexibility and shorter downtime to reconfigure their set-ups.

To ensure long-term profitability, manufacturing companies are introducing novel paradigms and digital approaches to monitor process executions (Morgan et al., 2021; Albanese et al., 2022). On the one hand, traditional paradigms such as flexible and dedicated manufacturing systems are distinguished by restricted capacity in reconfiguring themselves to meet a variable production with short life cycles (Bortolini et al., 2018). These limitations are mainly driven by two drivers. First, fixed systems structures require prolonged reconfiguration times or even prevent these modifications. A stark example is provided by dedicated manufacturing systems that are designed to satisfy high demands for a given product (Mehrabi et al., 2000). Second, the systems' structures need to achieve competing unitary costs and throughput times for a large variety of final goods (Xing et al., 2006). Reconfigurable manufacturing systems (RMS) overcome these limitations by dynamically adjusting their output capacities and system structure with respect to unforeseen market changes while ensuring competitive market costs (Bortolini et al., 2018; Mehrabi et al., 2000; Xing et al., 2006).

✉ Andrea Sbaragli
andrea.sbaragli@unitn.it

1 Department of Industrial Engineering, University of Trento, Via Sommarive 9, 38123 Trento, Italy

2 Department of Design, Production and Management, University of Twente, De Horst 2, 7522 LW Enschede, The Netherlands

Published online: 09 January 2025

On the other hand, traditional managerial tools are utterly inadequate to monitor these dynamic manufacturing environments since they strongly rely on human attention and commitment. The enabling technologies of Industry 4.0 trigger a digital transformation in industry operations by monitoring and improving in-plant productivity (Zheng et al., 2021). Although robotics and automation replaced the human factor in hazardous and repetitive tasks, human-centric environments still represent the vast majority of manufacturing settings (Goel and Gupta, 2020; Lu et al., 2022). Labor-intensive workplaces are often digitized by Internet of Things (IoT) technologies that mirror process executions in cyber spaces (Thiede et al., 2016). These distributed data-driven approaches enable performing process monitoring along with insights to manage and eventually redesign human-centric manufacturing systems. Within such a broad area of research, the Operator 4.0 concept demonstrates the tangible benefits of monitoring workers' operations to improve system performances (Romero et al., 2016; Pilati and Sbaragli, 2023). Among the different data acquisition layers, real-time locating systems (RTLS) technologies are increasingly adopted to detect human process interactions in low-standardized manufacturing environments (Pilati et al., 2024; Ruppert et al., 2018). The RTLS network leverages the anchors as reference points to define the coverage area and triangulate the unknown positions of workers equipped with wearable tags (Santoro et al., 2021). Regardless of the adopted IoT acquisition layer, cyber layers are required to leverage data streams to extract meaningful information about monitored processes and support plant supervisors' decision-making processes (Albanese et al., 2022; Thiede et al., 2022). Machine learning (ML) architectures are increasingly adopted due to their superior performance in automatically detecting recurrent patterns in data and developing insightful process-driven key performing indicators (KPIs) (Rude et al., 2018).

However, the Industry's 4.0 value proposition solely focused on processes' performances is not sustainable anymore in modern societies and manufacturing landscape (Ruppert et al., 2018). The Industry 5.0 paradigm fills this limitation by leveraging a human-centric value creation to mitigate the impact of two relevant external factors. First, the aging of the European population and the related increase in retirement age require to achieve socially inclusive manufacturing environments. The target is to design human-centric environments where desired in-plant performances are achieved with reduced operators' efforts. Second, market threats such as supply chain disruptions and raw material shortages demand the development of cyber layers that go beyond mere performance monitoring (Huang et al., 2022). These digital computational units should quickly reconfigure themselves to replicate process reconfiguration and reduce deployment times. In addition, algorithms' outputs are required to suggest operation managers optimal resource allocation and avoid unnecessary resource usage.

In this ever-evolving manufacturing landscape, this manuscript develops an original cyber-physical architecture to monitor human-centric RMS. In addition to the physical system under analysis, the architecture is conceptually composed of three layers. The IoT acquisition layer gathers positioning datastreams of workstations (WS) and operators leveraging a radio frequency-based RTLS. While WS' tags provide meaningful insight regarding the layout configuration of manufacturing systems, workers' motion patterns are fed into an ML-based cyber layer that performs set-up insensitive activity segmentation. This task is achieved through a two-step approach. First, a trained ML-based classifier assigns workers' operations to industrial resources (e.g., WS, storage locations) and detects logistic activities. Second, a resource-specific classifier further details the workers' operations into value-added and non-value-added. The main strengths of this approach are the ability to seamlessly reconfigure itself according to the state of the physical RMS system and the limited number of sensors adopted. These operator-driven outputs are stored in the last layer of this architecture, the Decision Support System. In this digital environment, customized callback functions are triggered to develop KPIs to monitor RMS from different viewpoints. While performance-oriented metrics evaluate the efficiency of manufacturing systems, another set of metrics evaluates industrial resources' interdependencies in production set-ups. For instance, the utilization ratio of industrial resources and operator-specific uptime operations enhance the visibility into processes' functioning and bottlenecks. Besides process monitoring, operation supervisors have pivotal information to manage and eventually design setup and batch-dependent manufacturing environments. This data-driven process minimizes process inefficiencies while ensuring desired in-plant performances with reduced efforts of a rapidly aging workforce. In addition, market-driven production volumes may be correlated with historical data to avoid systems over-allocations and ensure sustainable resource usage.

This original contribution is structured as follows. Section "Literature review" reviews the features of RMS along with the digital approaches to monitor these environments. The novelty of this work is discussed in section "Cyber-physical architecture", where the original cyber-physical architecture to monitor RMS sytems is presented. This digital solution is validated in an industrial-related pilot environment (section "Cyber-physical architecture validation"). The obtained manufacturing insights are discussed in section "Results". Finally, section "Conclusion" ends this work outlining the conclusions and further research opportunities.

Literature review

RMS adjust cost-effectively their design and functioning by re-configuring the hardware and software architectures of their interconnected entities (Mehrabi et al., 2000). However, this manufacturing system paradigm does not represent a sufficient condition to ensure companies' long-term profitability for a crucial aspect. The development of data-driven and digital solutions constitutes a necessary condition to monitor and optimize the evolving configurations of RMS. These methodologies can be broadly distinguished into two research areas (Bortolini et al., 2018; Napoleone et al., 2023).

On the one hand, heuristic and clustering-based optimization problems define objective functions to be either minimized or maximized given a set of constraints. For example, (Wang et al., 2016) proposes a clustering algorithm to create product families and the related production sequence to minimize processes' bottlenecks. The same target is achieved with multi-model assembly line balancing methods to minimize task reassignments among generic manufacturing systems' configurations (Tremblet et al., 2023). This mathematical approach reduces set-up times while preserving operations efficiency for different product families, consistently. Although the tangible benefits of managing and optimizing RMS, these solutions are often based on static parameters leading to potentially time-consuming algorithms' rearrangements. Another major limitation is not to consider and model the human factor stochastic behavior in processes' executions. Indeed, human-centric systems still play a pivotal role in the manufacturing ecosystem, where workers represent one of the most flexible resources in performing extremely value-added operations (Pilati and Sbaragli, 2023). This weakness is emphasized further by Industry 5.0 which promotes a human-centered value creation (Gladysz et al., 2023).

On the other hand, IoT technologies contribute to achieving cyber-physical architectures to monitor and manage RMS. These digital systems monitor and control physical environments by integrating embedded sensing units and computational algorithms (Liu et al., 2017). In this regard, several qualitative frameworks demonstrate the competitive advantages of leveraging cyber-physical architectures to support plant supervisors' decision-making process (Kazemi et al., 2023; Zheng et al., 2021; Bortolini et al., 2018). Additional remarks are directed towards the reconfigurability of cyber systems to obtain flexible computational algorithms able to minimize deploying times (Nayak et al., 2015). In the context of Industry 5.0, the ambition to digitize and support the human factor in RMS provides two main competitive advantages. First, operations supervisors gain a deeper understanding of in-plant operations by benefitting from further control parameters. Second, operators' skills and versatility are complemented to increase process performances, inclusively and sustainably (Rodriguez et al., 2015). However, research contributions have not developed and tested application-oriented cyber-physical architectures, where digital representations of the human factor enable to support the management of human-centric RMS (Napoleone et al., 2023; Touckia, 2023; Andersen et al., 2024). Indeed, many contributions target semi-automated environments, and thus operators benefit from the application of novel methodologies at the machines and system levels. For instance, cyber-physical architectures are widely adopted to improve material flow and reduce configuration set-ups, resulting in optimized workplaces for workers (Singh et al., 2020; Yi et al., 2018).

Although no contributions propose cyber-physical architectures to digitize the human factor in RMS, the validity of these digital and computational solutions is widely demonstrated in production environments (e.g., job shops and assembly lines) (Pilati et al., 2023; Thiede et al., 2016; Tran et al., 2021). Among the several enabling technologies, RTLS are increasingly gaining traction due to their ability to continuously acquire the indoor location of manufacturing assets within a coverage area (Pilati and Sbaragli, 2023; Thiede et al., 2021). RTLS networks present several methods to triangulate the position of tags and communication protocols with anchors (Sullivan et al., 2023; Santoro et al., 2021). Locating techniques can be broadly distinguished into fingerprinting and geometric, where the Time Difference of Arrival (TDoA) is widely adopted in industrial settings (Mazhar et al., 2017; Pilati et al., 2023). The TDoA estimates the dynamic positions of tags with respect to at least three active anchors using hyperbolic intersections (Mazhar et al., 2017). Similarly, communication protocols range from optical and infrared to radio frequency-based (Sullivan et al., 2023). The ultrawide band (UWB) one is the most accurate solution due to a high multipath resolution, granted by a bandwidth of at least 500 MHz (Mazhar et al., 2017).

The application of RTLS provides decision-makers enhanced visibility of human-centric manufacturing systems. For instance, (Sullivan et al., 2022) automates the Value Stream Map development. In addition to reducing data collection times, a cyber layer automatically identifies the dynamic human process interactions of the monitored system. Upon these outputs, process weaknesses can easily identified and thus addressed to ensure desired performance rates. Another valuable approach is to segment worker activities during working shifts. These insights are strategic to develop KPIs such as average production cycle and traveling times (Tran et al., 2021). However, these RTLS-informed cyber systems present two major weaknesses. First, the presented computational units are not validated with a ground truth data set to analyze the limitation in detecting human process interactions. Second, algorithms are based on geofencing manufacturing areas leading to high exposures in data outliers and reduced capabilities in detecting recurrent data patterns. In this regard, ML-based layers are increasingly deployed to monitor and support industrial operations. For instance, Pilati and Sbaragli (2023) develops a novel unsupervised clustering method (e.g., Industrial DB scan) to identify human process interaction, strategic to segment workers' activities during task executions. The same target is achieved by deploying an LSTM-based architecture to learn time series patterns in workers' indoor positions (Pilati et al., 2023). Therefore, Decision Support Systems display the utilization of industrial resources and the distribution of picking/deposit activities in storage areas over working shifts. An additional notable application is to safeguard the operational safety of human-centric environments. In particular, Islam et al. (2022) feeds UWB-based positions and breathing rates of workers into a specific set of esembled ML-methods (e.g., decision tree and Support Vector Machines) to promptly indentify dangerous scenarios and thus minimize rescue times. Besides these UWB and ML-based applications, the literature offers other applications to promote efficient process monitoring while supporting workers' capabilities. Cyber-physical architectures leverage different ML-based classifiers such as Support Vector Machines and tree structures (e.g., Random Forests) to support workers' quality inspections and reduce in-plant inefficiencies by promptly notifying process deviations (Jeffrey et al., 2024; Köttner et al., 2021).

Regardless the tangible benefits to manufacturing processes monitoring, these cyber-physical architectures are not tested and validated in RMS. This strong limitation results in cyber layers' reconfigurable capabilities leading to weak reliability and validity in constantly evolving industrial environments.

Manuscript contribution

To overcome the discussed limitations of the manufacturing landscape, this manuscript proposes a novel cyber-physical architecture to monitor and manage labor-intensive RMS performances and interdependencies. The key take-aways of this work are listed in the following.

- Layout and task insensitive cyber-physical architecture to minimize deploying time in monitoring human-centric RMS operations
- Low-invasive IoT acquisition layer based on RTLS to gather workers' motion patterns and industrial resources positions in production set-ups
- Sequential ML-based cyber layer to segment workers' activities (e.g., value-added and non-value-added working times)
- Decision support system and callback functions to display strategic KPIs to manage and eventually reconfigure processes design
- Validation of the proposed approach in an industrial-related pilot environment involving 40 workers and 8 production set-ups

Cyber-physical architecture

This section presents the innovative proposal of this manuscript. This architecture is developed to support decision-makers in managing and designing dynamic human-centric RMS. In particular, a specific set of enabling technologies is exploited to enhance these production environments with two different planning horizons. While the short-term one focuses on in-plant performances and interdependencies of production setups, the long mid-term planning horizon leverages simulation environments to iteratively assess the best layout configuration.

To meet these complementary goals, the cyber-physical architecture consists of four conceptual entities (Fig. 1). The first one targets whichever labor-intensive RMS that may adjust its functioning and layout configuration based on market demands and product batches. Instead of managing these complex environments based on plant managers' experience, an IoT acquisition layer is introduced to digitize processes' executions. While an RF-based RTLS acquires motion patterns and spatio-temporal information of workers and industrial resources (e.g., WS), machine interfaces mirror ongoing automation-based production processes. These data streams after specific pre-processing computations are fed into the third system's entity, the cyber-physical layer. Based on the desired planning horizon, two consecutive computations occur. On one hand, ML-based algorithms leverage positioning measurements to detect human-process interactions and thus segment operators' activities. Following a post-processing step, these outputs automatically generate KPIs upon which plant supervisors can monitor processes' functioning on the short-term horizon. On the other hand, discrete-based simulation models define iteratively sub-optimal production-specific layout configurations (Ghafoorpoor Yazdi et al., 2024). The main strength of both computational methods is their layout and task insensitivity. Indeed, these models quickly and seamlessly reconfigure based on WS positioning information. The obtained outputs are post-processed to generate KPIs in a decision support system (see Fig. 1). Both approaches provide detailed insights into processes' weaknesses suggesting to plant supervisors how to improve the efficiency and interdependencies of human-centric RMS while preserving social fairness. This work focuses on short-term planning and thus the remaining subsections in this Section target the yellow boxes in Fig. 1.

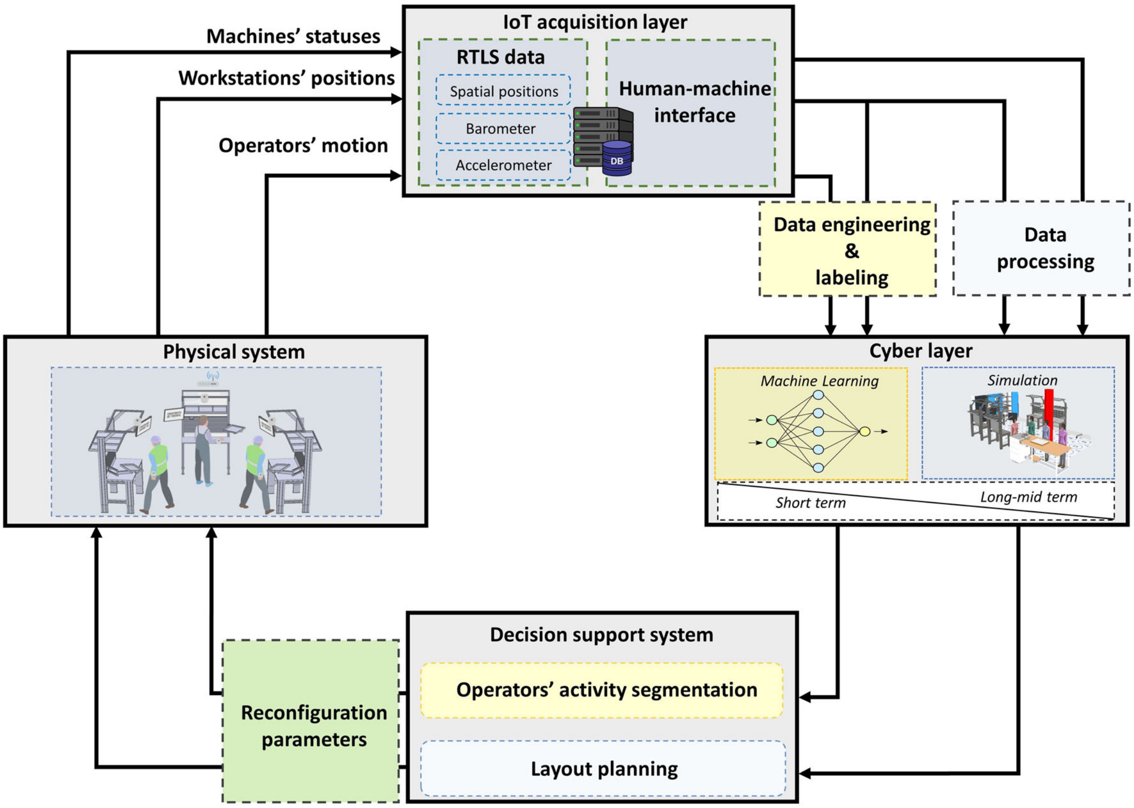

Fig. 1 Cyber-physical architecture to monitor and manage human-centric reconfigurable manufacturing systems (Color figure online)

IoT acquisition layer

The IoT acquisition layer leverages a UWB-based RTLS to acquire the motion patterns of workers' and WS' positions in various production set-ups. This spatio-temporal information is strategic to automatically classify workers' operations in human-centric manufacturing systems. In particular, the classification is distinguished by two objectives. First, layout-insensitive algorithms assign operators' activities to industrial resources and detect logistic activities (see section "Reconfiguration oriented computations"). Second, returned operators' activities are further divided into value-added and non value-added operations (see section "Operation oriented computations").

To achieve this challenging goal, workers wear anonymous tags on the wrist of their dominant hand to acquire the geometrical location as well as 3D acceleration profile. The positions and orientations of WS are acquired by placing two devices in known locations. In addition to the application, these moving entities differ in time resolutions. The datastreams of workers and WS are sampled at a frequency equal to 10 Hz and 1 Hz, respectively. At the same time, they share the same hardware design. These different time resolutions are chosen because workers' positions are way more dynamic than WS within production set-ups. Indeed, a single position for each WS is used in the data engineering step to pre-process the UWB-based dataset. The main advantages of these sensing units are compact size and a battery lifetime up to one year. In addition, additional sensors such as accelerometers are mounted on board. The $3D$ acceleration profiles may represent valuable parameters to learn and identify workers' activity during process executions (section "ML-based cyber layer"). Wearable tags are based on Decawave UWB radio modules and use Channel 5 with a bandwidth of 6500 MHz to exchange JSON messages with anchors using the mentioned refresh rates. In particular, the JSON bodies contain several measurements, namely 3D indoor positions, acceleration profiles, environmental parameters (e.g., temperature and pressure), and a tag ID. The displacement of anchors defines the IoT network reference system and the spatial manufacturing environment to be monitored. Six reference points are installed on the ceiling of an industrial-related pilot environment covering an area approximately equal to $70m^2$. anchors are based on Decavawe modules and an IEEE-compliant UWB transceiver. Connectivity and power supply are granted by a Power over Ethernet (PoE) switch resulting in a star network configuration. Finally, JSON messages are uploaded to an RTLS server (see Fig. 2) that determines the unknown position of moving tags through the TDoA geometrical method (Santoro et al., 2023).

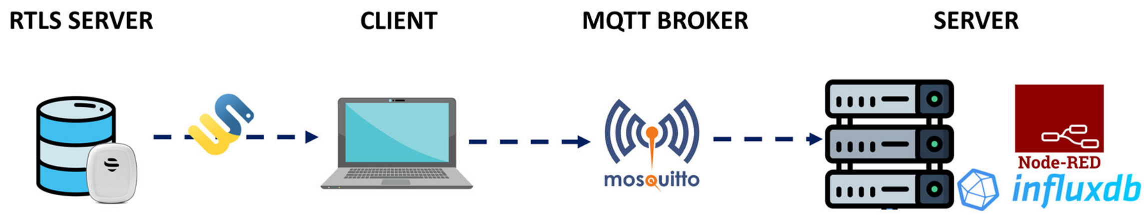

Fig. 2 Conceptual data flow of the IoT acquisition layer

Although this network configuration provides a stable data gathering of tagged entities, the RTLS server is a closed web-based application and thus prevents the development of customized algorithms. To overcome this hard limitation, Fig. 2 depicts the data flow of positioning information to an external physical server. In detail, the RTLS server is WI-FI connected to the Internet using a static IP address. By doing this, whichever client is connected to the Internet can retrieve real-time JSON data through WebSockets API. The client opens as many connections as the number of active tags using threads and locks to avoid unnecessary redundancies. Each connection and thus WebSocket communication is opened and managed by targeting the unique tag ID. Instead of storing data locally, the client node leverages the Message Queuing Telemetry Transport (MQTT) protocol and publishes positioning datasets in a TLS-encrypted Mosquitto Broker to ensure final users' privacy and avoid data leaks. Therefore, subscribers can authenticate the broker to retrieve JSON data, even in real-time or close to. Since the developed ML-based cyber layer operates with shift-based datasets, these messages are stored in a physical server connected to the Internet. Besides storing measurements in a time-series database (e.g., InfluxDB), a running node-red application parses the JSON messages. It is worth saying that the physical server can be remotely accessed by computational nodes through SSH connections.

ML-based cyber layer

This section details the ML-based computational steps to perform an activity segmentation of workers' tasks in human-centric RMS. In addition to detecting the performed activities, the cyber layer distinguishes value-added and non-value-added operations. A value-added activity occurs whenever workers perform process-driven activities in industrial resources (e.g., fastening screws). Otherwise, the worker status is idle which is a non-value-added operation. To achieve this challenging task, Fig. 3 depicts the closed-loop structure of acquired positioning data in the cyber layer, where the processing steps are associated with the corresponding outputs (e.g., see green-colored boxes). A preliminary overview of these computational steps is listed below:

- *Data engineering and labeling:* this step increases the dataset dimension by engineering additional features from the acquired motion patterns of workers. In particular, the dataset is distinguished by a relative coordinate system between workers' and industrial resources positions. This feature grants a high degree of adaptability to the computational layer in monitoring any system configuration.
- *Reconfiguration oriented computations:* this ML-based algorithm performs a layout and operator-insensitive classification of logistic activities and assignment to industrial resources (see section "Reconfiguration oriented computations").
- **Operation oriented computations:** this last ML-based step consists of a resource-specific approach to classify value-added and non-value-added operations (see section "Operation oriented computations").

These ML-based outputs are stored in a Decision Support System where callback functions develop KPIs to monitor the performances and the interdependencies of human-centered RMS (see section "Decision support system"). Based on this overview, the following subsubsections discuss the ML-based approach designed to mitigate limited and sparse datasets. Indeed, collecting a considerable amount of video-based ground truth in industrial environments may raise stakeholders' privacy concerns, from operators to labor unions.

Data engineering and labelling

This introductory step downloads the UWB-based datastreams of WS and workers in separate files from InfluxDB (see Fig. 2). Before designing the dataset features, an introductory step assesses the positions and orientations of WS for each production setup. The WS 2D positions are determined by averaging the acquired spatio-temporal data. This enables to mitigate the measurement noise of the adopted physical layer. The orientation on the z-axis of these entities is computed through the Arccos of motion vectors using as input both tags' positioning information. While the initial vector is constructed upon the initial positions of the workstation, the final vector underlines the setup location.

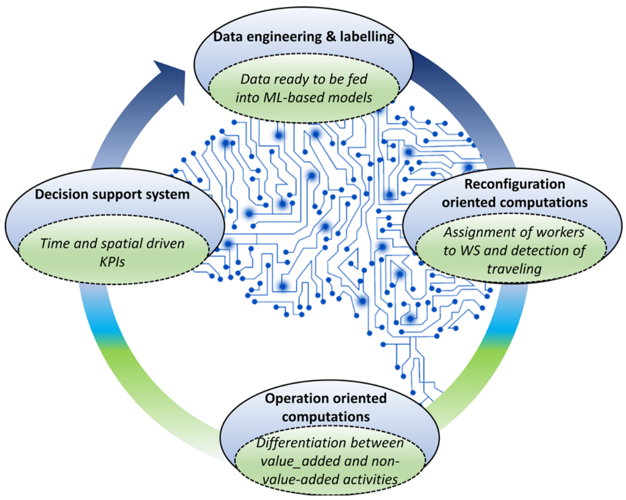

Fig. 3 Conceptual data mining of IoT data streams

At this point, the acquired workers' motion pattern undergoes data engineering and labeling processes. The data engineering step designs the dataset features to facilitate the learning capabilities of ML-based models. Besides raw absolute 2D indoor positions and 3D acceleration profiles parsed from the acquired JSON data streams, a dedicated script computes the relative distances with WS for each positioning frame and worker. This relative coordinate system provides ML-based classifier insensitiveness to production setups (e.g., see section "Reconfiguration oriented computations"). Operators' numbers and time-driven information (e.g., absolute clock for each production setup) complete the input features by establishing data relationships among parallel manual operations.

Following this data engineering step, ground truth data (e.g., video recordings) are analyzed to label workers' motion patterns, according to the operation performed. This multi-class classification involves as many labels as the number of WS in the manufacturing system. Traveling and idle states represent two further events to be classified. Based on this, the goal of the following ML-based computations is to perform an activity segmentation of manual task executions in human-centric manufacturing systems and thus offer multidimensional KPIs in a Decision Support Systems to evaluate the efficiency and interdependencies among industrial resources. Therefore, the first set of ML-based architectures leverages the described dataset features to automatically assign workers to a production resource and detect traveling states (section "Reconfiguration oriented computations"). Having as input these classifications, the second step designs WS-dependent algorithms to further detail the proximity of operators to resources into value-added and non-value-added operations (see section "Operation oriented computations").

Reconfiguration oriented computations

To automatically classify workers' proximities to industrial resources and traveling events regardless of production setup layouts, three ML-based algorithms are introduced and benchmarked with each other (e.g., LSTM, Industrial DB scan, and Random Forest). It is worth noting that classifiers' insensitiveness to setups is granted by the data engineering process (see section "Data engineering and labelling"), where a relative coordinate system between workers and WS positions is introduced. The following algorithms differ under different perspectives such as the hyper-parameters, and the learning type (e.g., supervised and unsupervised). While the LSTM-based architecture extracts valuable information in the time-series datasets, the Industrial DB scan detects high-density regions of spatio-temporal positioning points and the Random Forest classifies input data using decision trees. These algorithms are discussed in the following paragraphs and Appendix B lists the classifier-specific hyper-parameters to be optimized (see Tables 3, 4 and 6).

LSTM-based architecture: this supervised-based neural architecture follows the definition proposed in Pilati et al. (2023). LSTM architectures improve the standard formulation of recurrent neural for the vanishing gradient problem and better capture long-term patterns in time-series analysis (Pilati et al., 2023). Table 3 lists the set of hyper-parameters to be optimized. The core LSTM cell is distinguished by the input, forget, and output gates (see Fig. 4). The first updates the cell state by passing in a sigmoid function the input data at timestamp t and the previous hidden state. The closer the output is to 1 the higher informative value occurs in input data. The forget gate is responsible for selecting meaningful information in the cell state at timestamp t. The output of the sigmoid between the previous hidden state and the current input data is multiplied via the Hadamard product with the cell state. While outputs close to 0 suggest that the information can be discarded, values close to 1 indicate meaningful information. Therefore the cell state at timestamp t + 1 is given by the sum of potentially discarded information in the forget gate and the output of the input gate. Finally, the output gate is responsible for updating the hidden state to carry forward. Before feeding data streams into an LSTM-based architecture, engineered input data are processed by a sliding window algorithm. The dataset is divided into overlapping sliding windows of different sizes (see Table 3) and assigns the ground truth-based label to the last input data of the window. Sliding windows are shifted by one sample. In addition, three-dimensional tensors are generated having dimensions equal to the window size, the dataset features, and the batch size. This last parameter enables the computation of the mini-batch gradient and it is adopted to mitigate the vanishing problem during the network training (see Table 3). Each layer of the LSTM-based architecture has as many LSTM

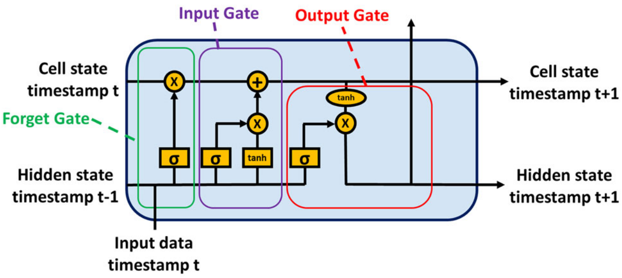

Fig. 4 LSTM cell

cells as the window size. The number of layers is an additional hyper-parameter to increase the architecture's ability to eventually learn complex patterns in input data. Considering an architecture with 2 layers, it is possible to approximate the network as a matrix where the number of rows is equal to 2 and columns equal to the window size. Where each matrix entry contains the LSTM cell in Fig. 4. For architecture with more than one layer, the dropout is often adopted to randomly offset some architecture neurons. This parameter offers a learning regularization and prevents the model's overfitting (see Table 3). Another relevant hyper-parameter in designing a robust LSTM-based architecture is the hidden state size (see Table 3). Contrary to the cell state that stores long-term information, the hidden state carries forward short-term information and overwrites at every timestep. The output of the LSTM cells of the last layer is fed into a fully connected neural network with an output size equal to the number of events to be classified. Finally, a normalized softmax activation function maps the multidimensional vector into the most significant class. After this forward propagation, the deep learning network computes the batch-based gradient using the cross-entropy function and updates the architecture weights and the learning rate based on the Adam optimization. Table 3 lists the initial learning rates.

Industrial DB scan: this unsupervised-based algorithm fills the limitations of its standard formulations with respect to time-sensitivity and an enhanced uncertainty mitigation approach (Pilati and Sbaragli, 2023). This clustering algorithm detects human-process interactions as high concentrations of spatio-temporal points in a defined layout region and assigns them to manufacturing systems' industrial resources (e.g., WS). The unsupervised algorithm does not need to be trained but requires the definition and a static assignment of five spatio-temporal hyper-parameters. Table 4 lists them with the related values intervals. First, ϵ and $NPts$ provide an initial clustering of human activities during production cycles. While ϵ defines the distance between geometrical points, NPts define the minimum number of points for each human-process interaction. This last parameter can be seen as a temporal constraint as well. In addition, spatio-temporal points grouped by ϵ and $NPts$ must be temporally consecutive and thus spaced by δt. Trivially, δt is equal to the sampling frequency of the adopted acquisition layer. However, these constraints do not adequately model the measurement noise and motion uncertainties of the IoT acquisition layer and workers, respectively. Indeed, it may be necessary to merge human-process interactions with each other to avoid skewed KPIs. For instance, let's define two consecutive human-process interactions (e.g., HPI_z and HPI_{z+1}). Each interaction is defined by a finite set of positioning points (e.g., $p_{i,z}$, where $i = 1, ..., I \; \forall z = 1, ..., Z$), a time window (e.g., TS_z^{start} and TS_z^{end}), and a geometric center (e.g., $O_z = \{Ox_z, Oy_z\}$). Therefore, HPI_z and HPI_{z+1} are merged together whether the Eq. (1) is true and at least one between Eqs. (2) and (3) is met.

$$TS_{z+1}^{start} - TS_z^{end} \leq \alpha \tag{1}$$

$$EuclideanDistance(p_{I,z}, O_{z+1}) \leq \beta \tag{2}$$

$$EuclideanDistance(p_{I,z}, p_{1,z+1}) \leq \phi \tag{3}$$

Table 4 shows the hyper-parameters considered in the previous equations, namely α, β and ϕ. While α depends on the average time spent to travel from HPI_z to HPI_{z+1}, β and ϕ are functions of the expected distance from consecutive process interactions.

Random forest: this supervised-based algorithm has a structure based on decision trees (Rigatti, 2017). The number of tree to be ensembled together is given by the hyper-parameter estimator number (see Table 6). Each tree computes the output class for any measurement in the training set. Several parameters influence the size and depth of these estimators. Among them, the minimum sample split defines whether a tree node is further split. The node is split if the number of samples in the node is less than the minimum (see Table 6). Otherwise, that node represents a leaf. The output of all decision trees is considered to determine the final output class. This process is known as aggregation and is based on majority voting. Trees models are diversified based on two different methods. First, bagging or bootstrap avoids model overfitting by reducing the sensitivity of training data. Therefore, each decision tree is provided with a sample of data with random replacements in between. Second, feature randomness differentiates the branches of trees' nodes enabling a better classification of datasets. Each decision tree chooses randomly a maximum amount of features based on $sqrt$ or $log2$ (see Table 6). Finally, the loss function to be minimized during the training process is given by the entry criterion in Table 6.

Operation oriented computations

This computation leverages the output of the previous classifiers bundled with the same feature space to train industrial resource-specific classifiers. In detail, assignments to industrial resources are further distinguished into value-added and non-value-added activities. Value-added operations groups events in which workers are performing manual tasks assigned in industrial resources. This computational step targets a binary classification and reduces algorithm complexity during the learning stage. In addition, it is particularly effective and practical in industrial environments where companies require ready-to-deploy solutions and privacy concerns combined with potential interference with processes' executions may limit extensive ground truth data gathering. Indeed, achieving representative datasets for human motions is a challenging task, especially in diversified workforces and heterogeneous manual operations. To achieve this ambitious aim, three different ML-based classifiers are benchmarked with each other, namely Random Forest, Gradient Boosting, and Support Vector Machine. The Random Forest algorithm discussion is not repeated since it follows the same formulation given in section "Reconfiguration oriented computations". In addition, Appendix B lists the classifier-specific hyper-parameters to be optimized (see Tables 6, 7 and 5).

Gradient boosting: similarly to the Random Forest, this supervised-based algorithm exploits ensemble learning method, where decision trees or estimators are trained as base learners and then leveraged to achieve input classifications (see Table 7). In addition, this classifier adopts the boosting techniques by learning in a sequential manner decision trees. Therefore, the initial and highly biased model is further complicated by adding more trees to minimize the residual error between actual and predicted values. The error is computed through the derivative of the squared logarithmic loss function with respect to the predicted value. In addition, the learning rate controls the importance of new trees added to the model during the classification process. Table 7 defines the set of hyper-parameters to be optimized, where the maximum features and the minimum sample splits follow the same definitions of the Random Forest classifier.

Support vector machine: this supervised-based algorithm is widely used for classification problems even though the training time exponentially increases with large datasets. The objective of this ML-based classifier is to define the optimal hyperplane that best differentiates input data streams' features. Data closest to the hyperplane are support vector points and their distances are the margins. The hyperplanes are computed based on similarity scores between pairs of training data. These scores are computed by choosing the preferred Kernel, where the Gaussian is one of the most popular (Keerthi and Lin, 2003). During the training process, two hyper-parameters need to be optimized (5). First, C can be seen as a model's regularization parameter by controlling the cost of misclassifications. Indeed, it trades off between correct classifications and the margin dimension. While to large value of C is associated with a small margin, the opposite scenario occurs with low C values. In this latter case, the probability of misclassifying data increases. Second, γ defines the influence level of a single training example with all the others. High values suggest a close influence between data points.

Decision support system

Based on the closed-loop computations of the cyber layer (see Fig. 3), Table 1 lists how the segmented workers' activities are stored before computing the multi-dimensional KPIs to monitor and manage human-centric manufacturing systems. In particular, the data engineering & labeling step acquires the JSON data of the UWB-based RLTS and then extracts the dataset features to be fed in the following two ML-based computations. While the reconfiguration oriented classifies logistic activities and assigns workers to industrial resources regardless the production setup, the operation oriented computation differentiates between value-added and non-value-added manual operations for each WS.

The first three columns of Table 1 outline the time-driven features of detected manual operations by storing the time window timestamps and the related duration. Working activities are classified by the operation and resource entries. While the first distinguishes between operation type (e.g., value-added and non-value-added), and traveling activities, the resource column specifies the industrial resource. The last column specifies the meters traveled between two temporally consecutive process interactions. Although this RTLS-based activity segmentation of workers' operations enriches the visibility of in-plant operations, it is impractical to effectively monitor the performances of human-centric RMS. To fill this gap, customized callback functions enable user-friendly decision-making facilitating innovative insights into the interaction of workers and workstations in flexible manufacturing systems. This is related to time and spatial aspects as well as the combination of both. Figure 5 provides an overview of considered KPIs and analysis items towards advanced decision support use cases for monitoring, planning, and improving manufacturing systems. For instance, industrial plant supervisors visualize the most utilized resources while understanding the allocation of operators to industrial resources. In general, these indicators extensively evaluate value-added activities to detect inefficiencies or bottlenecks in reconfigurable environments. Based on this level of detail, decision-makers have pivotal insights to reconfigure the process to achieve scheduled efficiencies. At the same time, the multi-dimensional from-to charts highlight the resources' interdependencies and the most exploited workers in material handling activities during production processes. This level of analysis is extremely beneficial for managers. First, they may aim to achieve fair

Table 1 Example of time-dependent working operation of workers within a production setup

Start	End	Duration [sec]	Operation	Resource	Distance [m]
10:06:26.47	10:06:46.09	19.62	Value-added	WS2	0
10:06:46.76	10:06:51.36	4.60	Non-value added	WS2	
10:06:51.59	10:06:53.83	2.15	Traveling	–	4.7
...	...	...	...	...	...
11:31:03.58	11:31:11.41	47.83	Value-added	WS4	0

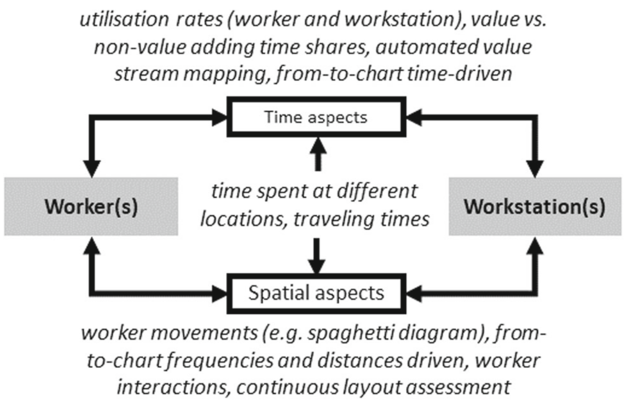

Fig. 5 Multidimensional KPIs embedded in the Decision Support System

RMS by equally involving workers in handling activities. Second, data-driven layout redesigns may increase the operational efficiency of human-centric RMS. Therefore, as clear advancements towards the state of the art, the suggested approach is flexibly adapting to changing manufacturing layouts and situations and enables an innovative breakdown of manufacturing activities (e.g. into value and non-value-adding time shares).

Cyber-physical architecture validation

This section validates the cyber-physical architecture to monitor human-centric RMS based on ML-based models. In particular, section "Industrial and reconfigurable use case" describes the industrial-related pilot environment where the workers' motion patterns and WS positioning information are acquired by a UWB-based RTLS. The obtained dataset consists of 8 manufacturing configurations, where a spinal prosthetic model is the final product to be assembled by exploiting various industrial workstations, operators, and task assignments (section "Feature-engineered workers' motion patterns"). Finally, the remaining sections "Performances of reconfiguration oriented computations" and "Performances of operation oriented computations" present the ML-based performances of the reconfiguration and operation oriented computations. These intelligent classifiers are trained and tested in a remote Jupiter server running in a Dell PowerEdge R740 with an Intel Xeon Platinum 8468H and RAM 256Gb.

Industrial and reconfigurable use case

The industrial-related pilot environment assembles a medical spinal prosthetic sample in different industrial resources, where one of them hosts a collaborative robot (see Fig. 6). WS are equipped with industrial screwdrivers and a fixed storage location that stocks components and fasteners. The manufacturing process requires fully assembling 3 final products by performing a wide range of tasks. Based on operators' experience, the entire production takes between 15 and 20 minutes. First, 8 blocks are glued together in pairs and thus drilled. Each block is distinguished by 4 holes. Subsequently, these blocks are fit into the prosthetic frames and screwed by industrial drivers. The third step screws together the prosthetic halves to achieve the final product. The production cycle ends with screwing quality tests. Based on this assembly process, 8 different production setups have been performed varying the number of WS, the task to workstation assignment, and the workers involved. Although this human-centric RMS may accommodate high product variances at affordable costs, a process monitoring based on supervisors' experience and human commitment results in unrepresentative analysis and thus underperforming decision-making.

To avoid these managerial weaknesses, the overall goal is to design a cyber-physical architecture that performs an activity segmentation of workers' tasks by distinguishing them into value-added and non-value-added, regardless of the different industrial setups during a pilot production of the medical prosthetic. In particular, the computational layer needs to be layout and operation-intensive to ensure easy-to-deploy in-plant monitoring. Based on this, a UWB-based RTLS acquires workers' motion patterns and industrial workstation locations in the production environment. As depicted in Fig. 7, six anchors are deployed in the ceiling of the monitored industrial-related pilot environment at known positions. These reference points are connected to a PoE switch that provides a stable power supply and a local network.

Based on the description of the industrial use case, the following subsection describes the feature-engineered dataset of workers' motion patterns during the spinal prosthetic assem-

Fig. 6 Static viewpoint of the industrial related reconfigurable pilot environment

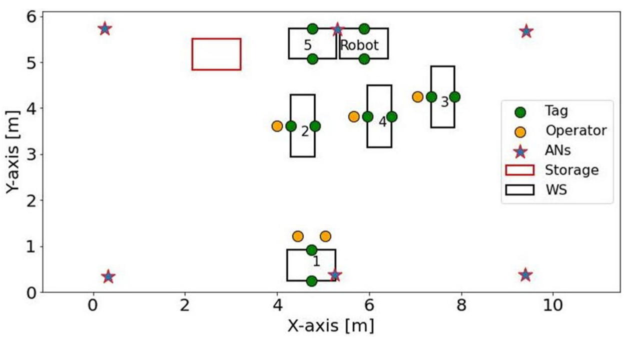

Fig. 7 Seventh production set-up

bly in 8 production setups. Each manufacturing configuration is implemented twice on different working days.

Feature-engineered workers' motion patterns

This subsection describes the operator-specific datastreams that are fed into the ML-based cyber layer. The global dimension of the dataset is equal to 814065 samples. These time-driven motion patterns are acquired in 8 production setups involving a total of 41 different workers. In this regard, Table 8 in Appendix C specifies the setup-dependent WS' absolute 2D positions and the number of operators. Since less than 25% and 40% of production setups involve 5 and 6 workers, the vast majority of input data is held by the first four operators. Table 9 lists the gathered input data for each operator number. The collected video-based ground truth enables frame-oriented data labeling and thus 9 different classes are adopted to distinguish workers' operations during production processes. This supervised and time-consuming process deeply affects the deployment time of ML-based models. A possible and viable solution to slash down data labeling times is to run a time-dependent script that assigns real-time labels to workers' operations based on keyboard entries of

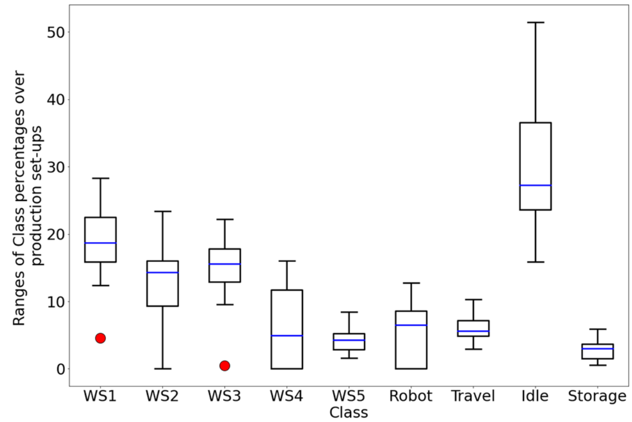

Fig. 8 Dataset classes distributions in percentage

numbers. However, this approach requires the supervision of each worker-dedicated running script and thus it is not implemented due to the shortage of researchers. The classes from $WS1$ to $WS5$ underline process-specific working activities in these WS. Similarly, $Robot$ and $Storage$ suggest human-automation interactions and the picking of raw materials and components (e.g., fasteners). The $Idle$ class is introduced to group all non-value-added operations regardless of the spatio-temporal positions within 8 production setups. Figure 8 outlines using boxplots the distributions of the discussed industrial classes among production setups. The $Idle$ state represents the majority of events in this highly unbalanced dataset with a median value equal to 27.27%. The maximum and minimum values account for 51.48% and 15.87%, respectively. While the maximum is connected to the second production setup during the first recording day, the lower bound is registered in the fourth production setup and second recording day. The higher bound is markedly affected by the Operator 6 operations that are non-value-added for the 88.89% of his/her production time. The other most populous classes are $WS1$, $WS2$ and $WS3$ peaking at 28.3%, 23.42% and 22.23%, respectively (see Fig. 8).

Considering the challenging target of designing a configuration and operation-insensitive architecture, an additional data investigation targets the distribution of acceleration profiles. Therefore, $Working$ and $Idle$ represent the newly formed operators' states under analysis. In particular, the $Working$ state groups workers' value-added datastream in whichever workstation and production set-up. Figure 9 shows the 3D distributions of acceleration profiles in the mentioned operator states. It is worth noting that these distributions have overlapping patterns and the underlying one and multi-way ANOVA tests are distinguished by really weak p-values. This scenario confirms the null hypothesis and may be driven by two main factors. First, the dataset dimension fails to generalize both workers' motion patterns and the performed manual operations. However, it may be difficult to extensively acquire ground truth information in industrial use cases due to privacy concerns (Pilati and Sbaragli, 2023). Second, the IoT acquisition layer is required to increase the sampling frequency to obtain higher resolutions in acceleration motion patterns (Liu et al., 2020).

To mitigate the dataset sparsity and the low resolution of acquired accelerations, the proposed ML-based cyber layer mines value inside data using a two-step approach. First, state-of-the-art algorithms assign workers to industrial resources (e.g., WS and storage location) and detect logistic activities (see section "Reconfiguration oriented computations"). However, this computational step approximates any workstation proximity to value-added operations. Therefore, the second computational step fills this gap by performing a binary classification between $Working$ and $Idle$ states (see section "Operation oriented computations"). Six different ML-based classifiers are trained to learn meaningful motion patterns from $WS1$ to the robotic workstation. The performances of these two computational steps are described in the following sections "Performances of reconfiguration oriented computations" and "Performances of operation oriented computations".

Regardless of the different targets of these computational algorithms, the dataset is split into three sets, where the validation has a share equal to the 70% of the dataset and the remaining two (e.g., validation and test) accounts for 15%. Production set-ups in recording days are assigned entirely to one of these sets and are not duplicated. In particular, the test set contains datastreams of the 7-th production setups during the second recording day. Figure 7 shows the layout configuration of this setup as well as the number of workers. In addition, the bold entry in Table 8 of Appendix C outlines the absolute workstation positions and number of workers for this production setup. In particular, the $WS1$ dedicated workers glue and drill the blocks to be inserted in prosthetic frame halves. Then, the righter worker of $WS1$ is in charge of moving finished products in $WS2$, $WS3$, and $WS4$ where prosthetic halves are fully assembled. The production process ends using the robotic arm to screw together the prosthetic halves to achieve the final product. This process is remotely controlled from $WS5$ where an automated final inspection of products is performed.

Performances of reconfiguration oriented computations

This subsection validates the first step of the ML-based computations (see section "Reconfiguration oriented computations"), where the hyper-parameters optimized classifiers are benchmarked with each other. Before going through the performance metrics (Fig. 10 and Table 10 in Appendix D), it is worth describing the adopted data splitting approach. On the one hand, the supervised learning approaches (e.g., LSTM-based architecture and Random Forest) are trained on 70% of the entire dataset. The remaining input data are equally split into the validation and the test sets. In particular, production setups are randomly assigned to the mentioned dataset splits, preserving their temporal dependence. The seventh production setup during the second recording day and the second setup on the first recording day belong to the test set. On the other hand, the Industrial DB scan does not require training and thus the following performances are evaluated both on the 7th production set-up and on the entire dataset. Table 10 in Appendix D depicts these performances, where values between brackets relate to the entire dataset. Regardless of the classifier, three different metrics (see Eq. from (4) to (6)) benchmark the classification performances of the presented ML-based algorithms.

$$Precision = \frac{TP}{(TP + FP)} \tag{4}$$

$$Recall = \frac{TP}{(TP + FN)} \tag{5}$$

$$Micro\ F1 - score = \frac{TTP}{TTP + \frac{1}{2} * (TFP + TFN)} \tag{6}$$

The first two class-dependent metrics are functions of true positives (TP), false positives (FP), and false negatives (FN). While Precision measures results' relevancy, the Recall indicates how many truly relevant results are returned. The Micro F1 score is chosen as a global metric due to its ability to better reflect imbalanced data distributions (see Fig. 8). Where TTP, TFP, and TFN are derived by summing up the related class-dependent metrics (e.g., TP, FP, and FN).

Based on the intrinsic differences of ML algorithms, Fig. 10a shows promising Micro F1 scores for all classifiers. In particular, the Random Forest and Industrial DB scan represent the worst and best-performing approaches accounting for 0.82 and 0.87, respectively. However, this global metric fails to highlight the class-specific strengths and weaknesses of these models. To fill this gap, the performance evaluation of this computational stage starts with the Pytorch-coded LSTM-based architecture. Based on the hyper-parameters in Table 3, the optimal network configuration is iteratively assessed. Batch, window, and hidden sizes are equal to 64, 128, and 256. The architecture is distinguished by solely one LSTM layer and thus the dropout is not introduced. Finally, the learning rate is equal to $1e^{-4}$. Figure 10b shows the Cross-Entropy-based loss for both the training and validation set over 300 epochs. While the training loss starts at 1.21 its profile over epochs decreases to meet convergence at 0.01, the validation Cross-Entropy opens at 2.62, and the loss is distinguished by fluctuations over training epochs. In addition, after reaching the local minima equal to 0.34 at epoch 49, the validation curve increases to 0.72. Since this scenario may indicate model overfitting, Fig. 10c depicts the Micro F1 scores within data splits over model epochs. Although the

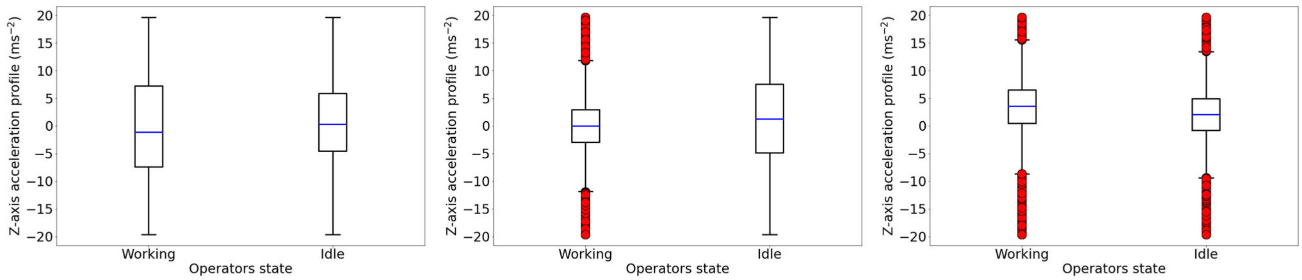

(a) X-axis acceleration distribution (b) Y-axis acceleration distribution (c) Z-axis acceleration distribution

Fig. 9 Distributions of 3D acceleration profiles of UWB-based tags on operators' hand

training F1 score is approximately equal to 1 from epoch 94 on-wards, the validation and test set have similar profiles and do not shrink. The 111-th model epoch with related learned weights maximizes the test F1 score accounting for 0.86 (see Fig. 10a). Figure 10d shows the confusion matrix related to this model epoch, where the main diagonal contains the correct classified datastreams. Before analyzing the confusion matrix, it is worth stating that this computationally expensive architecture is distinguished by an inference time equal to 90 sec for each training epoch and a test time approximately of 38 sec.

The confusion matrix suggests that the vast majority of dataset classes present low misclassification dispersion (e.g., FP and FN). Indeed, WS apart from $WS4$ and the $Storage$ present Micro F1 scores ranging from 0.82 to 0.98 (see Table 10). However, WS4 and Travel classes are distinguished by underperforming F1 scores accounting for 0.63 and 0.48, respectively (see Table 10). On the one hand, the Precision and Recall of the fourth workstation are equal to 0.84 and 0.51 leading to class underestimation due to a high amount of FN. This scenario is driven by a limited representation of this class in the dataset. Indeed, the class shares range from 1.31% to 15.72% within production setups (see Fig. 8). In addition, half of production environments do not exploit $WS4$ during the prosthetic assembly. On the other hand, the $Travel$ class shows low values for Recall and Precision. This scenario is driven by narrowed production setups where the UWB-based RTLS is stressed with short distances between manufacturing WS (see Table 8).

The second classifier is the Industrial DB scan. The model's hyper-parameters are shared and have the same values as the first algorithm definition and validation proposed in (Pilati and Sbaragli, 2023). In particular, ϵ, $NPts$ and δt are equal to 0.17 m, 15 positioning points and 10 Hz. The measurement noise and motion uncertainty-driven hyper-parameters, namely α, β, and ϕ account for 1 second and 0.5 m. Based on this hyper-parameters selection (see Table 4), the Micro F1 score of the 7th production set-up is equal to 0.87. Figure 10e shows the related confusion matrix for this targeted multiclass problem. This clustering method presents a computational time equal to 72 sec for each operator in the considered production setup. Similarly to the LSTM-based architecture, the F1-score of industrial resources from $WS1$ to $WS5$ ranges from 0.80 to 0.95. It is worth noting that the $WS4$ F1-score accounts for 0.94, markedly higher than the one obtained with the LSTM-based architecture (see Table 10). A different scenario emerges for the $Storage$ class where the neural network architecture outweighs this density-based method. Indeed, an underperforming Recall value provides an F1 score equal to 0.54. This low statistic is driven by a relevant limitation of the Industrial DB scan. The definition of static hyper-parameters may not reflect different positioning accuracies of the UWB-based IoT acquisition layer in manufacturing systems' local regions. In the targeted industrial-related pilot environment, such a scenario emerges for x and y values ranging from 0 to 3 and from 3.75 to 6 m, respectively (see Fig. 7). Both classifiers are distinguished by weak capabilities in detecting logistic activities in the mentioned industrial-related pilot environment due to narrowed distances between workstations (see Tables 10, 8).

The last classifier to detect reconfiguration-oriented operations is the Scikit-learn-coded Random Forest. The optimal hyperparameters configuration is found using the grid-search algorithm. This sub-optimal configuration is distinguished by a number of estimators and minimum sample splits equal to 70 and 3, respectively. In addition, the optimal criterion and maximum features are given by $entropy$ and the $sqrt$. Figure 10f depicts the related confusion matrix that provides a Micro F1 Score equal to 0.82. The described training and test times are equal to 140 and 15 sec, respectively. Although this classifier is the worst performing in detecting manufacturing operations, $WS1$ and $WS5$ F1 scores outweigh the previous two computational methods. Overall, this statistic for the other classes is satisfactory apart from $WS4$ and $Travel$. While the first confirms the limitations already analyzed with the LSTM-based architecture, the logistic activities are a shared weakness of all benchmarked intelligent algorithms (see Table 10).

After this quantitative discussion on class-specific performances, the LSTM-based architecture is chosen over the

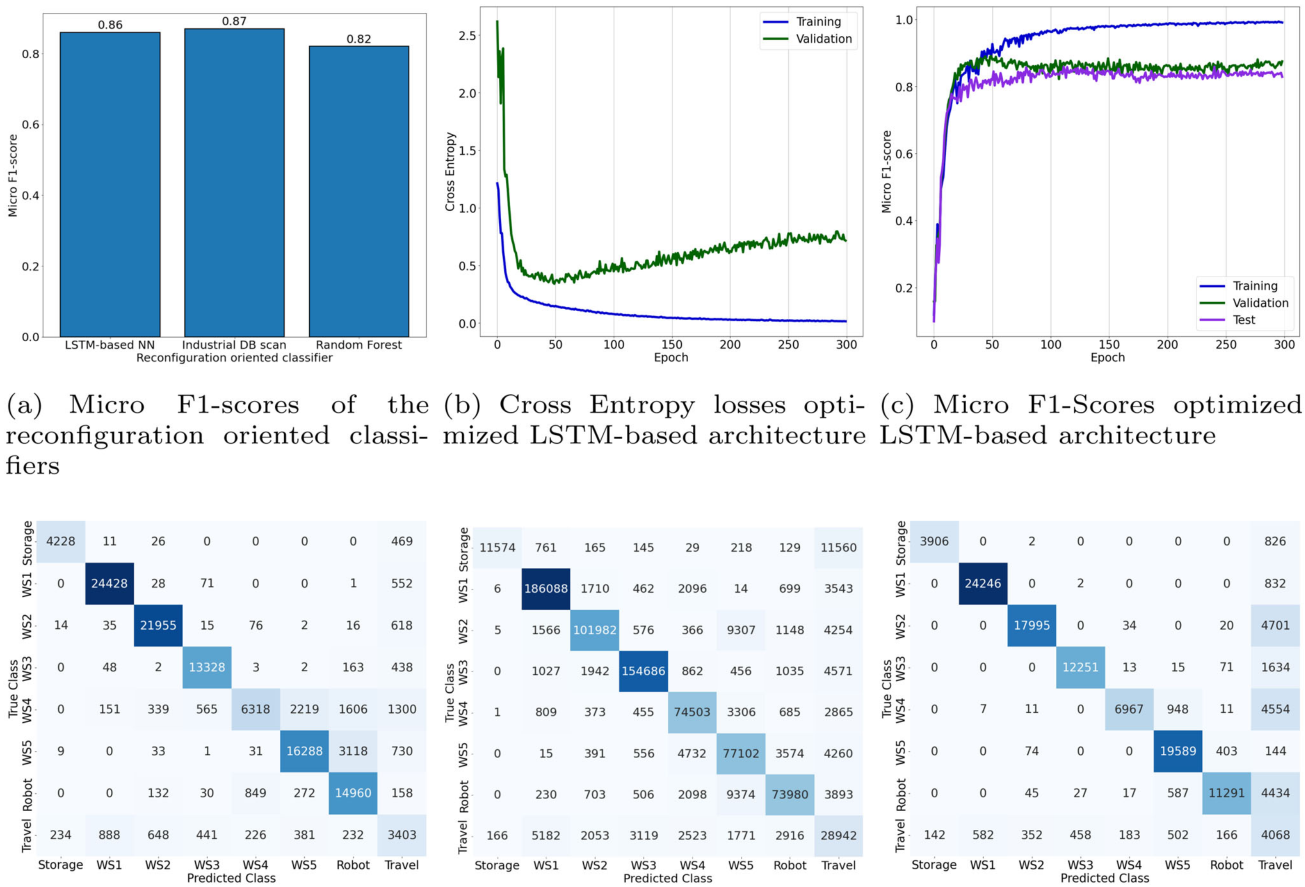

(a) Micro F1-scores of the reconfiguration oriented classifiers

(b) Cross Entropy losses optimized LSTM-based architecture

(c) Micro F1-Scores optimized LSTM-based architecture

(d) Confusion matrix optimized LSTM-based architecture

(e) Confusion matrix optimized Industrial DB scan

(f) Confusion matrix optimized Random Forest

Fig. 10 Performances of ML-based classifiers of reconfiguration-oriented computations

Table 2 Qualitative benchmark of reconfiguration oriented ML-based methods

Classifier	Training	Deployment time	Number of hyper-parameters	Dataset size
LSTM-based architecture	Yes	High	High	Large
Industrial DB scan	No	Low	Low	Small
Random forest	Yes	Low	Medium	Medium

Industrial DB scan for a main reason. It is preferable to achieve a better Micro F1-score for the *Storage* class rather than in $WS4$ which is hardly used in the considered manufacturing process (see Fig. 10). Despite the adopted model selection to maximize classification performances, the following Table 2 provides an additional and useful distinction of the benchmarked ML-based classifiers. The listed features may guide practitioners in implementing the most adequate model based on their needs and requirements. For instance, the Industrial DB scan represents the most effective solution with a limited dataset and related ground truth baseline information. In addition, this density-based computational method does not require training and thus the deployment time solely relies on the identification of a sub-optimal hyper-parameters values set.

Performances of operation oriented computations

This subsection discusses the performances in classifying working and idle activities, given the industrial resource (see section "Operation oriented computations"). To do so, three grid search optimized (see bullet point in Appendix D) ML algorithms are trained using a resource-specific dataset with test sets' dimensions varying from 7.3 to 17.5% (e.g., $WS5$ and $WS2$ represent the lower and upper bound). This computational step considers solely data streams acquired

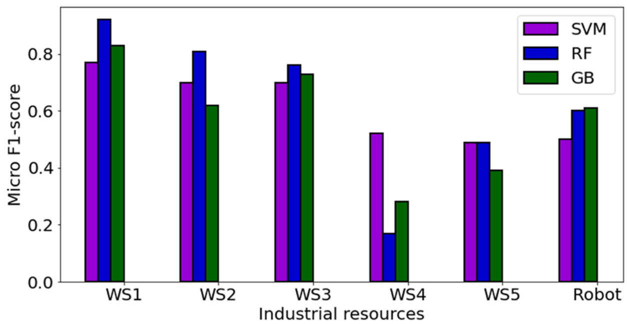

Fig. 11 Micro F1-scores of the operation oriented classifiers

during the second recording day due to reduced exposure to motion uncertainty in workers' assembly activities. Considering computational times, the Support Vector has markedly higher statistics compared to the other two models. Indeed, the Gradient Boosting and the Random Forest are distinguished by mean and standard deviation training times equal to 35 and 5 sec, respectively. The same statistics for the Support Vector account for 11.5 and 2.2 minutes. The related mean and standard deviation for the inference shrinks to 2.5 minutes and 70 sec.

Figure 11 shows the industrial resources-centered (e.g., from $WS1$ to $Robot$) Micro F1-scores in identifying value-added and non-value-added activities. The acronyms SVM, RF, and GB refer to Support Vector Machine, Random Forest, and Gradient Boosting methods to limit space. Overall, the first three WS are distinguished by markedly higher Micro F1-scores compared to the remaining others. This scenario is driven by the nature of tasks allocated to WS. Indeed, the most manual-intensive activities such as drilling blocks and screwing them into the model's frame are usually assigned to $WS1$, $WS2$, and $WS3$. Based on this, two algorithms are selected to differentiate workers' status (e.g., $Working$ and $Idle$) in industrial resources. While the Random Forest is the most appropriate method for the first three workstations, Gradient Boosting shows better capabilities in the remaining workstations where operators' motion patterns are limited.

Starting the discussion with the most manual-intensive industrial resources, the Random Forest Micro F1-score values of $WS1$, $WS2$, and $WS3$ are equal to 0.92, 0.81, and 0.76, respectively (see Fig. 11). These promising statistics are also reflected by analyzing the resources and operator state-driven Precision, Recall, and F1-score metrics (see Table 11 in Appendix D). In particular, the Random Forest algorithm outperforms the other methods showing deltas up to 0.49. A stark example is provided by the Recall values of non-value-added activities in WS1 (see Table 11).

A different scenario emerges for the remaining industrial resources from the fourth WS to the robotic one. Indeed, the Support Vector Machine and the Random Forest show superior Micro F1-scores compared to the Gradient Boosting algorithm (see Fig. 11). For instance, considering $WS4$, the Support Vector accounts for 0.52 compared to 0.28 of the Gradient Boosting. However, Table 11 suggests that both Random Forest and Support Vector Machine classifiers overfit the data set. In detail, the value-added class for $WS4$ and $WS5$ is never recognized. Based on this, the Gradient Boosting is leveraged as the most adequate classifier to evaluate the operator state in these WS. Despite this selection, the detection capabilities are not satisfactory for two main aspects. First, 3D acceleration profiles present overlapping distributions among $Working$ and $Idle$ classes, as already pointed out during the dataset description (see section "Feature-engineered workers' motion patterns"). Second, these industrial resources are distinguished by pretty static workers' motion patterns. For example, operators' activities are limited to interaction with the machine interface and highly assisted quality checks in the robotic and fifth WS. To conclude this classifier and resource-oriented discussion, Fig. 16 in Appendix D shows the confusion matrices for each resource and chosen ML-based algorithm.

Benefitting from these sequential ML-based computational steps, a time and label- oriented algorithm segments workers' activities as shown in Table 1. Sequentially, callback functions leverage these outputs to achieve KPIs to monitor the efficiencies and interdependencies of production set-ups.

Results

After the performance validation of the designed ML-based cyber layer, this section discusses the managerial insights and implications of monitoring with IoT technologies task executions in human-centric RMS. The following KPIs generated by dedicated Python scripts discuss the performances and interdependencies of the 7th production set-up during the second recording day lasting 16 minutes approximately.

This production setup employs 5 workers to fully assemble 3 spinal prosthetic models resulting in 5.45 minutes/product. Figure 12 shows the utilization ratio of industrial resources as a function of workers' value-added operations over the monitored shift (e.g., ST stands for Storage and ANs for anchors).

The most saturated resources of this production set-up are the first three WS. While WS1 peaks at 77.82%, WS2 and WS3 are distinguished by utilizations equal to 72.31 and 70.22%, respectively. This scenario is driven by the task allocation to WS. Indeed, WS1 hosts manual gluing and drilling of blocks. Subsequently, blocks are moved into three parallel WS (e.g., WS2, WS3, and WS4) that fit two wooden blocks each into the prosthetic model halves. The analyzed KPI demonstrates that WS2 and WS3 are preferred over WS4. This last resource is used as a jolly workstation showing a utilization ratio lower than 30%. Based on

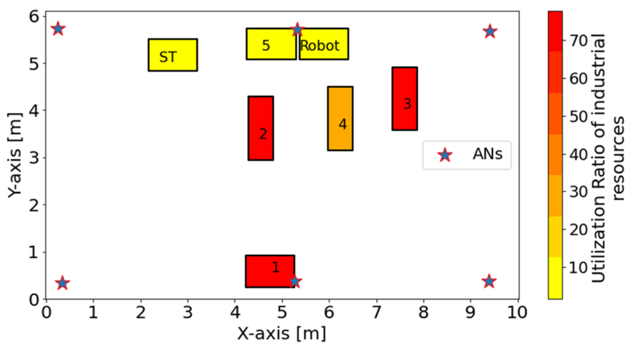

Fig. 12 Utilization of Industrial resources over the monitored shift

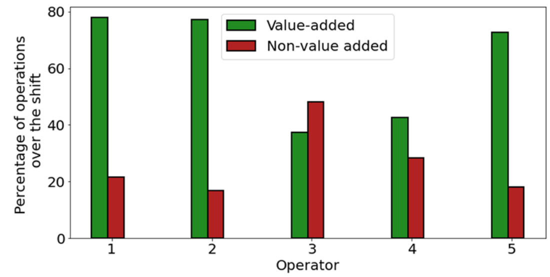

(a) Distribution of operator-centric operations

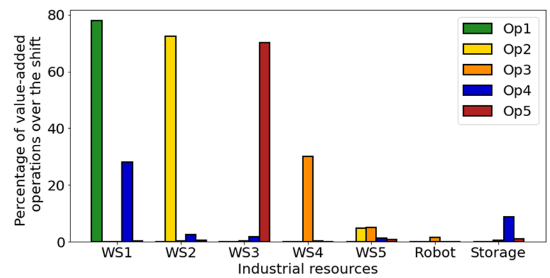

(b) Distribution of value-added operations among operators and resources

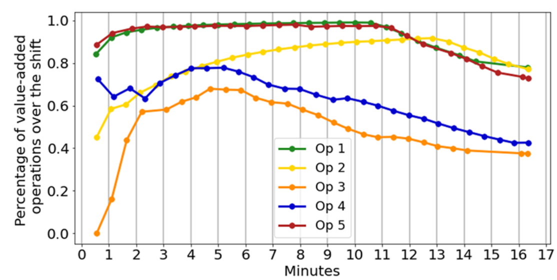

(c) Operator specific percentage of value-added operations over the shift

Fig. 13 Activity segmentation of workers operations

this first insight, plant supervisors should identify the over-allocation of resources that negatively impact both economic indicators and potential distances traveled by workers to perform production cycles. In this regard, it would be recommended to reduce the number of workstations and eventually assign an additional jolly operator either to WS2 or WS3 to lower potential bottlenecks and operators' efforts to meet required takt times. The remaining industrial resources are distinguished by low utilization lower than 10%. The quality control in WS5 and the human-robot interactions represent quick and less labor-intensive tasks. Although this KPI highlights potential redundant WS in production set-up, it falls short in segmenting workers' operations over the shift. Figure 13a–c fill this gap by highlighting the distribution of value-added and non-value-added operations as well as the operators' assignments to WS. First, Fig. 13a outlines the operator-centric distributions of value-added and non-value-added operations as a function of the shift duration. This KPI is extremely effective in pointing out the most undersaturated workers in performing process-related activities. While Op1, Op2, and Op5 register shares of value-added operations greater than 72%, Op3 and Op4 are distinguished by values equal to 37.42 and 42.57%, respectively. Although this first overview may suggest an over-allocation of workers to the production setup, further metrics are required to carefully analyze this working shift.

Second, Fig. 13b depicts the value-added activities performed by operators among the seven industrial resources of this production set-up. This metric enables to differentiate operators' tasks. While Op1 and Op2 value-added operations never below 72% are limited to WS1 and WS3, the remaining operators are way more dynamic showing interactions with multiple resources. Op3 and Op4 represent striking examples and provide additional details into the process's functioning. On the one hand, the distribution of Op3 value-added activities suggests that low productivities of WS4 are integrated with quality checks and robot interactions. On the other hand, Op4 interacts with almost all industrial resources of the manufacturing system, where an 8.77% of time is reserved by picking activities from the storage location. This insight may suggest that this worker is also in charge of manual material handling operations among industrial resources.

Third, Fig. 13c further details workers' value-added operations by evaluating their share in production routines using a time resolution of 30 sec. This KPI notifies plant supervisors of potential workers' over-allocations to production set-ups. Although three operators (e.g., Op1, Op2, and Op5) are distinguished by shares of value-added operations greater than the 80% for the majority of the production shift, Op3 and Op4 hardly exceed the 70%. In particular, Op3 is the least involved in value-added activities. Benefitting from these KPIs, decision-makers may reduce the workforce size and re-distribute Op3 tasks to the remaining others, most likely to Op2 and Op5 that share similar operations.In general, workers' over-allocations are detrimental to in-plant perfor-

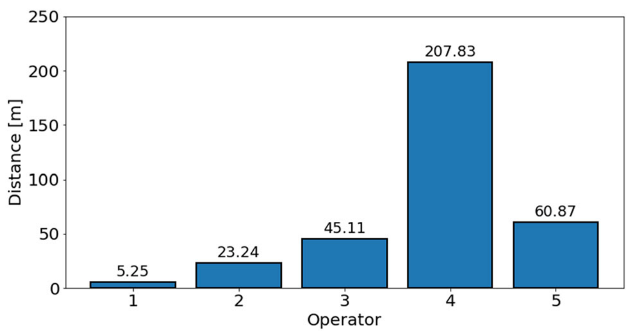

Fig. 14 Distances traveled by operators over the shift

mances. First, stagnant outputs per unit of time and operators may penalize workers' commitments and awards during gamification approaches. Second, incorrect systems design in manufacturing systems with interconnected job shops may drastically affect companies' market competitiveness.

Besides process-oriented manual operations, it is pivotal to focus on traveling events to discuss the interdependencies among industrial resources. A top-down approach is established to achieve this purpose. Figure 14 shows the distances traveled by monitored workers over the working shift. Op4 travels 3 up to 20 times the distances of his/her colleagues, overcoming 200 m during the shift. This statistic is consistent with the distribution of value-added activities among operators and resources (see Fig. 13b). Indeed, Op4 interacts with almost all industrial resources and spends approximately 10% of his/her working time in the storage location. This distance-dependent statistic negatively affects the social inclusiveness and sustainability of the considered human-centric RMS. This scenario is driven by two main factors. First, an over-allocation of resources with non-optimal positions may lead to longer logistic activities. This can be mitigated by the long-mid term planning horizon of the architecture as discussed in (Ghafoorpoor Yazdi et al., 2024). Second, plant supervisors should be encouraged to redistribute logistic activities among the workforce. This point assumes further relevance when manually handled products present considerable weight and risk scores of ergonomic indices (e.g., NIOSH and EAWS) represent valuable weights to be fed into objective functions (Yaoyuenyong and Nanthavanij, 2008).

However, not accessing the operator-centric travel activities fails to highlight the most involved resources of production set-ups. Figure 15 fills this gap by depicting the multidimensional from to charts of Op4 in the frequency, time, and spatial domains. It is worth noting that a valid traveling activity between two industrial resources must contain at least 20 indoor positions. This choice is made to limit the cyber layer's limitations in detecting this event combined with an in-depth process analysis. Starting to analyze the frequency domain, Fig. 15 outlines the amount of traveling events or flows among industrial resources.

It is interesting to note that the 3 out of 5 flows from the storage location are directed to WS3. The same amount of flows from WS3 are then directed to WS2. Analyzing the global picture, WS2 and WS3 are distinguished by a higher amount of incoming and outgoing flows compared to WS4. This flow distribution confirms the utilization ratio of WS4 in this production set-up. Figure 15a confirms that Op4 handles the replenishment of WS2, WS3, and WS4 while feeding to them the blocks to be screwed in the prosthetics halves. Scaling the same approach to the entire workforce, other material handling activities may be detected and thus analyzed. For instance, Op1 presents solely one travel activity from the storage to WS1. This value points out accurate management of wooden blocks because it suggests that the required wooden blocks to produce 3 final products are moved at once. The logistic activities toward the final stages of the production cycles (e.g. robotic workstation and quality check in WS5) are managed by Op3 and thus are not discussed further. To better analyze process functioning and potential inefficiencies, Fig. 15b, c link the discussed flows with the aggregated distances traveled and the time spent. For example, 12.7 sec and 18.3 m that are registered during the 3 flows between the storage location and WS3 may be reduced by changing the replenishment logic. The advantage of knowing a priori the desired output rate should encourage decision-makers to design an adequate buffer size for each workstation. This would enhance the material handling times and distances by avoiding multiple and unnecessary interactions with the storage. Considering the parallel operations of the three industrial resources (e.g., WS2, WS3, and WS4), a shared buffer location may be designed as well to limit obstruction among operators during task executions. Another valuable layout modification is to bring closer WS2 and WS3. By doing this, Op4 would slash down the 14.1 sec and the 23.5 m during three traveling events. The same approach can be used with WS1 in bringing it closer to WS2 and WS3.

To conclude, the designed cyber-physical architecture can effectively enhance the visibility of human-centric RMS through different multi-criteria variables. On the one hand, performance-driven metrics suggest sub-optimal allocation of WS and workers to production setups. This contributes to improving manufacturing systems' economic metrics while reducing operators' efforts during manual task executions. In addition, these metrics may be complemented by additional data such as market demands and production batches to create families of production setup designs. On the other hand, investigation of logistic activities suggests potential disadvantaged workers and valuable inputs to heuristic optimization to re-balance traveled distances during production cycles. In addition, operator-centric from to charts pinpoint the interdependencies of industrial resources constituting valuable inputs to re-layout production environments.

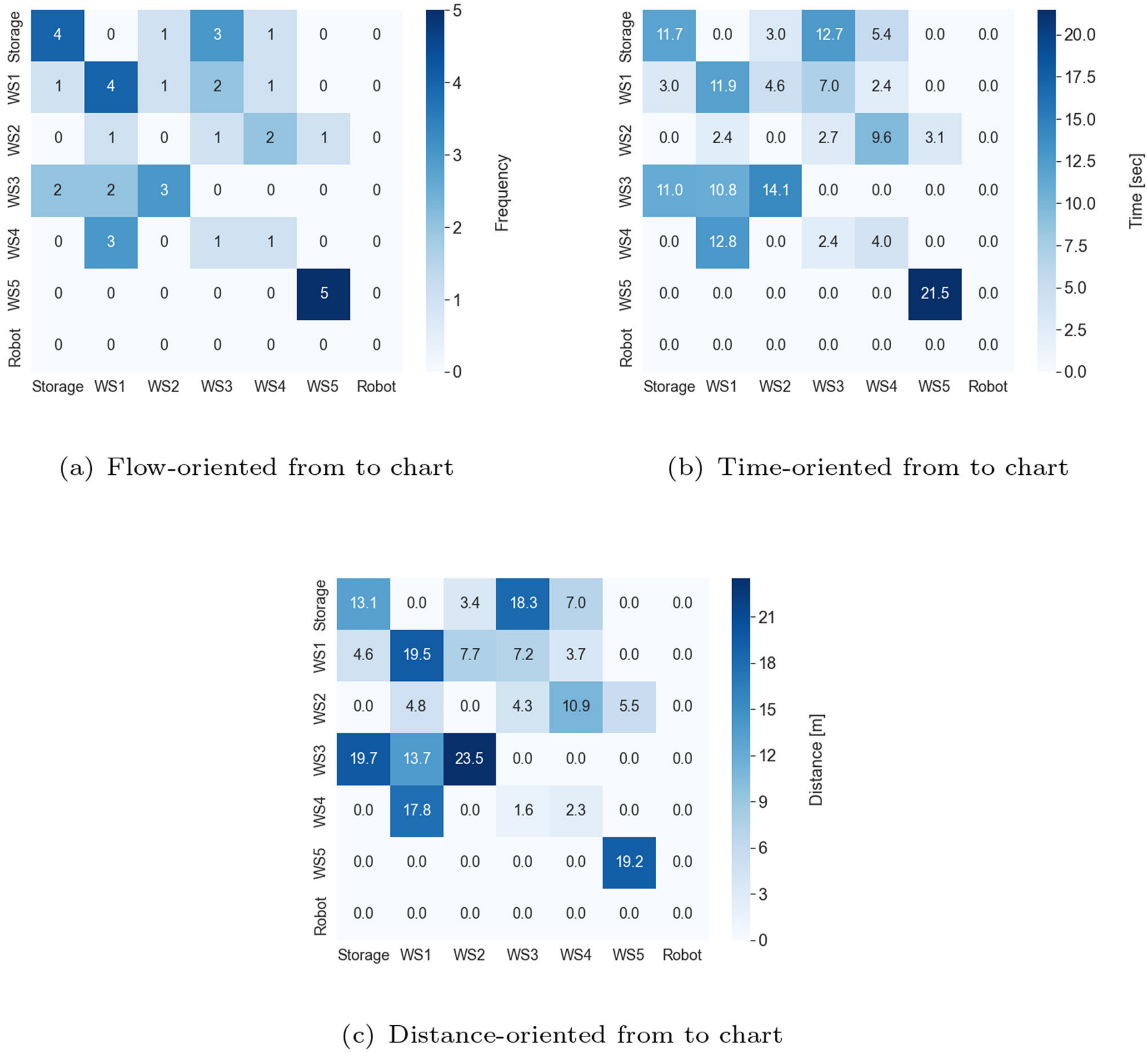

Fig. 15 Multidimensional from to charts of operator 4

Conclusion

The ever-evolving market demands are posing serious challenges to modern manufacturing systems' operational efficiency. To cope with this threat, RMS offers high production flexibility at competing unitary costs. These modular and variable environments involve a joint effort of manufacturing entities and human resources. Conventional managerial tools and decision-maker experiences fall short of ensuring stable in-plant performances. For this purpose, cyber-physical architectures represent a necessary condition to monitor and manage the systems' reconfiguration along with the workforce's stochastic behavior.

Based on this, this work presents a cyber-physical architecture that leverages a UWB-based RTLS network to acquire the motion patterns and the indoor location of workers and industrial resources, respectively. These data streams are fed into a layout and task-insensitive ML-based cyber layer to segment workers' activities over working shifts. The designed cyber layer consists of two computational steps. First, the reconfiguration oriented computations automatically detected workers' proximities to industrial resources (e.g., WS) and traveling events. Second, the operation oriented computation further details operators' proximities into value-added and non-value-added activities. These operator-driven outputs are stored in a Decision Support System where customized callback functions develop strategic KPIs. Benefitting from these multi-criteria variables, plant supervisors monitor the in-plant efficiencies of production set-ups and if necessary trigger process reconfigurations.

This digital application is tested in an industrial-related pilot environment involving 40 workers and 8 production set-ups. In particular, the LSTM-based architecture results in the best reconfiguration oriented classifier, showing F1-scores in assigning workers to industrial resources greater than 0.82. The major weaknesses of this method are the assignment to the fourth WS for lack of training data and the detection of logistic activities due to narrowed distances among resources and the human factor's intrinsic uncertainty. At the same time, the operation oriented computations leverage two ML-based algorithms. While the Random Forest is the most performing in labor-intensive task, the Gradient Boosting is chosen to detect manual activities in semi-automated scenarios.

Following the validation of the ML-based algorithms, the managerial implications of monitoring human-centric RMS are discussed using the 7th production set-up of the dataset. In particular, the low utilization ratio of WS4 suggests to decision-makers that this industrial resource is redundant. Similarly, the number of workers may be reduced. Indeed, the value-added operations of Op3 and Op4 hardly exceed 70% during the monitored shift. The analysis ends by discussing the interdependencies among industrial resources. Multi-dimensional from to charts of Op4 are presented to highlight the patterns of the traveling events in handling materials to WS2, WS3, and WS4.

Further research should focus on different viewpoints. First, it is pivotal to improve the cyber-layer capabilities in detecting traveling non-value-added activities, especially for semi-automated production activities. Additional wearable sensors may be adopted to better capture manual activities and walking patterns among close industrial resources. Second, a human digital twin should be developed to monitor process executions in close-to real-time and model forecasting functions to notify workers of the next production tasks to be performed. By doing this, plant supervisors might promptly identify and manage process disruptions while assisting workers during task executions. Finally, two points target the decision support system. While Large Language Models might automatically discuss the proposed KPIs and derive actionable feedback and eventually reconfiguration strategies, a Graphical User Interface or dashboard may achieve a user-friendly monitoring process by preventing managers from interacting with low-level Python scripts.

Acknowledgements The authors express deep gratitude to the University of Twente Teaching Assistants who supported the activities in arranging an accurate experimental campaign.

Author Contributions Conceptualization, ST, AS, PGY, FP; software, AS; case study, AS, PGY; validation, AS, PGY; formal analysis, AS; investigation, ST, AS, PGY, FP; resources, PGY, ST; data curation, AS; writing-original draft preparation, AS; writing-review and editing, ST, AS, PGY, FP; visualization, ST, AS, FP; supervision, ST, PGY, FP; project administration, ST, PGY; funding acquisition, ST, PGY. All authors have read and agreed to the published version of the manuscript.

Funding Open access funding provided by Università degli Studi di Trento within the CRUI-CARE Agreement. This work has been partially funded by the SMART-ER seeds SPA1 of the ECIU consortium.

Declarations

Conflict of interest The authors declare that they have no Conflict of interest.

Appendix A

This appendix contains the list of acronyms defined in the manuscript.

RMS	Reconfigurable manufacturing systems
IoT	Internet of things
RTLS	Real time locating systems
ML	Machine learning
KPIs	Key performing indicators
WS	Workstation
RFID	Radio frequency identification
TDoA	Time difference of arrival
UWB	Ultrawide band
JSON	JavaScript object notation
PoE	Power over internet
API	Application programming interface
MQTT	Message queuing telemetry transport
SSH	Secure shell
TLS	Transport layer security
LSTM	Long short term memory

Appendix B

This appendix lists the relevant sets of hyper-parameters to be optimized during the reconfiguration and operation-oriented computations (see sections "Reconfiguration oriented computations" and "Operation oriented computations"). Please appreciate the ML-specific parameters in the following tables (Tables 3, 4, 5, 6, 7, 8).

Table 3 LSTM hyper-parameters

Parameter	Value
Window size	50, 128, 256
Layer	1, 2
Hidden size	100, 128, 256
Learning rate	$1e^{-2}$, $1e^{-3}$, $1e^{-4}$
Batch size	64, 128
Dropout	0, 0.3, 0.5

Table 4 Industrial DBSCAN hyper-parameters

Parameter	Value
ϵ	[0.1, 0.6] m
NPts	[10, 100] points
δt	[10 100] Hz
α	[1, 10] sec
β	[0.1, 2] m
ϕ	[0.1, 2] m

Table 5 Gaussian support vector hyper-parameters

Parameter	Value
C	1, 10, 100, 1000
γ	0.001, 0.01, 0.1, 1, 10

Table 6 Random forest hyper-parameters

Parameter	Value
Estimators number	50, 70, 100, 150
Criterion	Gini, entropy
Maximum features	sqrt, log2
Minimum sample split	2, 3, 4

Table 7 Gradient boosting hyper-parameters

Parameter	Value
Estimators number	50, 70, 100, 150
Loss	Logarithmic
Learning rate	$1e^{-1}$, $1e^{-2}$, $1e^{-3}$
Maximum features	sqrt, log2
Minimum sample split	2, 3, 4

Table 9 Operator-based dataset dimension

Operator	Number of input data
1	92, 435
2	94, 147
3	99, 320
4	90, 947
5	68, 380
6	27, 118

Appendix C

This appendix contains additional insights related to production setups. In particular, the 2D indoor positions of WS and the dimension of the feature-engineered workers' motion pattern are outlined in the following Tables 9.

Table 8 Absolute positions of industrial resources in different production setups

Setup	Workers	WS1		WS2		WS3		WS4		WS5		Robot	
		X	Y	X	Y	X	Y	X	Y	X	Y	X	Y
1	6	4.57	3.35	4.43	1.22	6.76	4.13	6.56	2.34	6.23	1.03	6.37	3.12
2	6	4.40	2.79	6.23	4.29	6.17	1.39	4.7	5.12	9.82	3.26	8.44	3.36
3	5	8.20	3.27	6.35	3.96	6.63	1.84	4.94	1.06	4.29	1.73	4.05	3.08
4	4	5.00	3.11	6.24	4.23	6.10	2.03	4.51	5.21	8.87	3.61	9.01	1.86
5	5	4.50	3.31	4.32	1.29	6.23	4.51	5.85	2.08	8.25	3.77	8.04	1.75
6	4	4.57	3.35	4.43	1.22	6.76	4.13	6.56	2.34	6.23	1.03	6.37	3.12
7	**5**	**4.75**	**0.91**	**4.30**	**3.61**	**7.34**	**4.25**	**5.97**	**3.82**	**4.78**	**5.07**	**6.30**	**5.70**
8	6	4.53	3.37	6.13	2.46	6.34	4.21	4.56	0.88	8.72	3.19	7.98	3.42

Bold values are related to the 7th production set-up. Results are based on this layout (see Fig. 7)

Appendix D

This appendix further details the performances for both reconfiguration and operation-oriented computations. Therefore, Precision, Recall, and F1 scores are computed for each dataset class and ML-based classifier. It is worth noting that the Industrial DB scan performances include both metrics for the 7th production set-up and the entire dataset. Where values in brackets represent the performances over the dataset (Fig. 16; Tables 10, 11).

The following bullet point lists the grid-search optimized set of hyper-parameters related to the ML classifiers of the operation oriented computations:

- *Support vector machine:*
  - C: 1

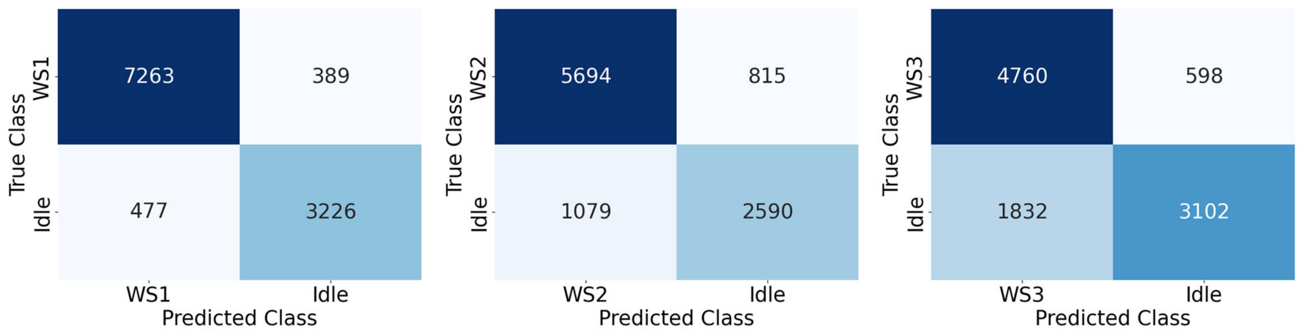

(a) Random Forest classification between WS1 and Idle states (b) Random Forest classification between WS2 and Idle states (c) Random Forest classification between WS3 and Idle states

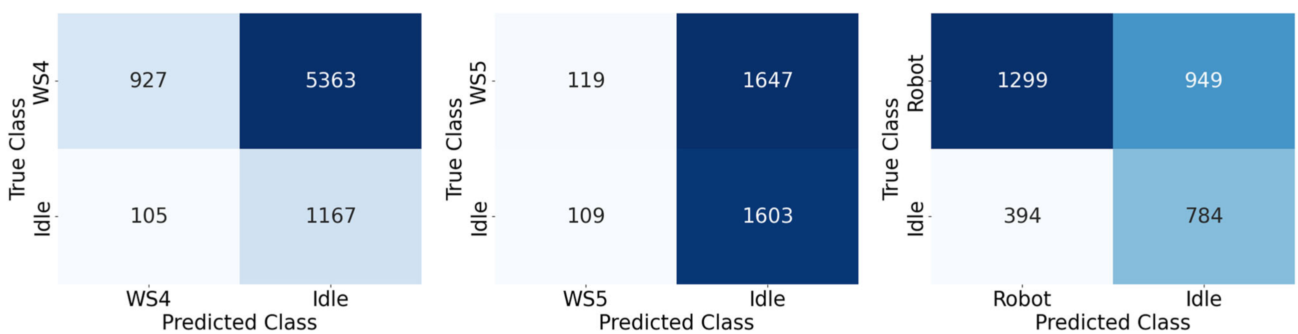

(d) Gradient Boosting classification between WS4 and Idle states (e) Gradient Boosting classification between WS5 and Idle states (f) Gradient Boosting classification between Robot and Idle states

Fig. 16 Confusion matrices of the best performing classifiers for the operation oriented computations

Table 10 Performances of optimized classifiers for reconfiguration oriented computations

Class	LSTM architecture			Industrial DB scan			Random forest		
	Precision	Recall	F1-score	Precision	Recall	F1-score	Precision	Recall	F1-score
$WS1$	0.96	0.89	0.92	0.95 (0.93)	0.96 (0.92)	0.95 (0.92)	0.98	0.97	0.97
$WS2$	0.96	0.97	0.96	0.96 (0.97)	0.94 (0.90)	0.95 (0.93)	0.97	0.79	0.87
$WS3$	0.92	0.95	0.94	0.93 (0.90)	0.86 (0.88)	0.89 (0.85)	0.96	0.88	0.92
$WS4$	0.84	0.51	0.63	0.96 (0.90)	0.94 (0.95)	0.95 (0.92)	0.97	0.56	0.71
$WS5$	0.85	0.81	0.83	0.76 (0.70)	0.85 (0.90)	0.80 (0.79)	0.91	0.97	0.93
$Robot$	0.74	0.91	0.82	0.88 (0.81)	0.81 (0.88)	0.85 (0.84)	0.94	0.69	0.80
$Travel$	0.44	0.53	0.48	0.45 (0.5)	0.62 (0.70)	0.52 (0.58)	0.19	0.63	0.29
$Storage$	0.94	0.89	0.92	0.98 (0.90)	0.47 (0.45)	0.64 (0.60)	0.96	0.83	0.89

Table 11 Performances of optimized classifiers for operation oriented computations

Industrial resource	Classifier	Working			Idle		
		Precision	Recall	F1-score	Precision	Recall	F1-score
$WS1$	Support vector machine	0.76	0.95	085	0.81	0.38	0.53
WS1	**Random forest**	**0.94**	**0.95**	**0.94**	**0.89**	**0.87**	**0.88**
$WS1$	Gradient boosting	0.80	0.99	0.88	0.97	0.47	0.64
$WS2$	Support vector machine	0.72	0.86	0.79	0.63	0.41	0.5
WS2	**Random forest**	**0.84**	**0.87**	**0.86**	**0.76**	**0.71**	**0.73**
$WS2$	Gradient boosting	0.81	0.54	0.65	0.49	0.77	0.59
$WS3$	Support vector machine	0.65	0.92	0.76	0.84	0.57	0.60
WS3	**Random forest**	**0.72**	**0.89**	**0.80**	**0.84**	**0.63**	**0.72**
$WS3$	Gradient boosting	0.68	0.89	0.78	0.83	0.56	0.66
$WS4$	Support vector machine	0.82	0.55	0.66	0.16	0.43	0.23
$WS4$	Random forest	0	0	0	0.17	1	0.28
WS4	**Gradient boosting**	**0.90**	**0.14**	**0.25**	**0.18**	**0.92**	**0.30**
$WS5$	Support vector machine	0	0	0	0.49	1	0.66
$WS5$	Random forest	0	0	0	0.48	1	0.65
WS5	**Gradient boosting**	**0.52**	**0.07**	**0.12**	**0.49**	**0.94**	**0.65**
Robot	Support vector machine	0.62	0.64	0.63	0.26	0.24	0.25
Robot	Random forest	0.68	0.72	0.70	0.41	0.37	0.38
Robot	**Gradient boosting**	**0.77**	**0.57**	**0.66**	**0.45**	**0.66**	**0.53**

Bold highlights the most performing classifier for each industrial resource (*WS*1, *WS*2, etc.)

  - γ: 0.001
- *Random forest:*
  - Estimators number: 70
  - Criterion: $entropy$
  - Maximum features: $sqtr$
  - Minimum sample split: 3
- *Gradient boosting:*
  - Estimators number: 100
  - Learning rate: $1e^{-}1$
  - Maximum features: $sqrt$
  - Minimum sample split: 2

References

Albanese, A., Nardello, M., Fiacco, G., & Brunelli, D. (2022). Tiny machine learning for high accuracy product quality inspection. *IEEE Sensors Journal, 23*(2), 1575–1583.

Andersen, R., Napoleone, A., Andersen, A. L., Brunoe, T. D., & Nielsen, K. (2024). A systematic methodology for changeable and reconfigurable manufacturing systems development. *Journal of Manufacturing Systems, 74*, 449–462.

Bortolini, M., Galizia, F. G., & Mora, C. (2018). Reconfigurable manufacturing systems: Literature review and research trend. *Journal of Manufacturing Systems, 49*, 93–106.

Ghafoorpoor Yazdi, P., Sbaragli, A., Peters, L., Pilati, F., & Thiede, S. (2024). Cyber physical system for reconfigurable learning factories: Combining 3d simulations, reconfigurable layouts and real-time locating systems. In *Conference on learning factories* (pp. 28–35). Springer.

Gladysz, B., Ta, Tran, Romero, D., van Erp, T., Abonyi, J., & Ruppert, T. (2023). Current development on the operator 4.0 and transition towards the operator 5.0: A systematic literature review in light of industry 5.0. *Journal of Manufacturing Systems, 70*, 160–185.

Goel, R., & Gupta, P. (2020). Robotics and industry 4.0. In *A roadmap to industry 4.0: Smart production, sharp business and sustainable development* (pp. 157–169).

Huang, S., Wang, B., Li, X., Zheng, P., Mourtzis, D., & Wang, L. (2022). Industry 5.0 and society 5.0-comparison, complementation and co-evolution. *Journal of Manufacturing Systems, 64*, 424–428.

Islam, F. B., Lee, J. M., & Kim, D. S. (2022). Smart factory floor safety monitoring using UWB sensor. *IET Science, Measurement & Technology, 16*(7), 412–425.

Jeffrey, N., Tan, Q., & Villar, J. R. (2024). Using ensemble learning for anomaly detection in cyber-physical systems. *Electronics, 13*(7), 1391.

Kazemi, Z., Rask, J. K., Gomes, C., Yildiz, E., & Larsen, P. G. (2023). Movable factory-a systematic literature review of concepts, requirements, applications, and gaps. *Journal of Manufacturing Systems, 69*, 189–207.

Keerthi, S. S., & Lin, C. J. (2003). Asymptotic behaviors of support vector machines with Gaussian kernel. *Neural Computation, 15*(7), 1667–1689.

Köttner, L., Mehnen, J., Romanenko, D., Bender, S., & Hintze, W. (2021) Process monitoring using machine learning for semi-automatic drilling of rivet holes in the aerospace industry. In *Production at the leading edge of technology: Proceedings of the 10th congress of the German Academic Association for production technology (WGP), Dresden, 23–24 September 2020* (pp. 497–507). Springer.

Liu, Y., Peng, Y., Wang, B., Yao, S., & Liu, Z. (2017). Review on cyber-physical systems. *IEEE/CAA Journal of Automatica Sinica, 4*(1), 27–40.

Liu, S. Q., Zhang, J. C., & Zhu, R. (2020). A wearable human motion tracking device using micro flow sensor incorporating a micro accelerometer. *IEEE Transactions on Biomedical Engineering, 67*(4), 940–948.

Lu, Y., Zheng, H., Chand, S., Xia, W., Liu, Z., Xu, X., Wang, L., Qin, Z., & Bao, J. (2022). Outlook on human-centric manufacturing towards industry 5.0. *Journal of Manufacturing Systems, 62*, 612–627.

Mazhar, F., Khan, M. G., & Sällberg, B. (2017). Precise indoor positioning using uwb: A review of methods, algorithms and implementations. *Wireless Personal Communications, 97*(3), 4467–4491.

Mehrabi, M. G., Ulsoy, A. G., & Koren, Y. (2000). Reconfigurable manufacturing systems: Key to future manufacturing. *Journal of Intelligent Manufacturing, 11*, 403–419.

Morgan, J., Halton, M., Qiao, Y., & Breslin, J. G. (2021). Industry 4.0 smart reconfigurable manufacturing machines. *Journal of Manufacturing Systems, 59*, 481–506.

Napoleone, A., Andersen, A. L., Brunoe, T. D., & Nielsen, K. (2023). Towards human-centric reconfigurable manufacturing systems: Literature review of reconfigurability enablers for reduced reconfiguration effort and classification frameworks. *Journal of Manufacturing Systems, 67*, 23–34.

Nayak, N. G., Dürr, F., & Rothermel, K. (2015). Software-defined environment for reconfigurable manufacturing systems. In *2015 5th international conference on the internet of things (IOT)* (pp. 122–129). IEEE.

Pilati, F., Sbaragli, A., & Papini, G. P. R., & Capuccini, P. (2023). An artificial neural network architecture to classify workers' operations in manual production processes. In *International conference on flexible automation and intelligent manufacturing* (pp. 805–812). Springer.

Pilati, F., Sbaragli, A., Ruppert, T., & Abonyi, J. (2024). Goal-oriented clustering algorithm to monitor the efficiency of logistic processes through real-time locating systems. *International Journal of Computer Integrated Manufacturing*, *37*(10–11), 1359–1375.

Pilati, F., & Sbaragli, A. (2023). Learning human-process interaction in manual manufacturing job shops through indoor positioning systems. *Computers in Industry, 151*, 103984.

Rigatti, S. J. (2017). Random forest. *Journal of Insurance Medicine, 47*(1), 31–39.

Rodriguez, L., Quint, F., Gorecky, D., Romero, D., & Siller, H. R. (2015). Developing a mixed reality assistance system based on projection mapping technology for manual operations at assembly workstations. *Procedia Computer Science, 75*, 327–333.

Romero, D., Stahre, J., & Wuest, T., Noran, O., Bernus, P., Fast-Berglund, Å., & Gorecky, D. (2016). Towards an operator 4.0 typology: a human-centric perspective on the fourth industrial revolution technologies. In *Proceedings of the international conference on computers and industrial engineering (CIE46), Tianjin, China* (pp. 29–31).

Rude, D. J., Adams, S., & Beling, P. A. (2018). Task recognition from joint tracking data in an operational manufacturing cell. *Journal of Intelligent Manufacturing, 29*, 1203–1217.

Ruppert, T., Jaskó, S., Holczinger, T., & Abonyi, J. (2018). Enabling technologies for operator 4.0: A survey. *Applied Sciences,8*(9), 1650.

Santoro, L., Nardello, M., & Brunelli, D., & Fontanelli, D. (2021). Scale up to infinity: The uwb indoor global positioning system. In *2021 IEEE international symposium on robotic and sensors environments (ROSE)* (pp. 1–8). IEEE.

Santoro, L., Nardello, M., Brunelli, D., & Fontanelli, D. (2023). Uwb-based indoor positioning system with infinite scalability. *IEEE Transactions on Instrumentation and Measurement, 72*, 1–11.

Singh, P. P., Madan, J., & Singh, H. (2020). A systematic approach for responsiveness assessment for product and material flow in reconfigurable manufacturing system (RMS). *Materials Today: Proceedings, 28*, 1643–1648.

Sullivan, P., Ghafoorpoor Yazdi, P., & Thiede, S. (2023). Real time locating systems (RTLS)—An enabling technology to support engineering education within learning factories. Sebastian.

Sullivan, B. P., Yazdi, P. G., Suresh, A., & Thiede, S. (2022). Digital value stream mapping: Application of UWB real time location systems. *Procedia CIRP, 107*, 1186–1191.

Suzić, N., Forza, C., Trentin, A., & Anišic, Z. (2018). Implementation guidelines for mass customization: Current characteristics and suggestions for improvement. *Production Planning & Control, 29*(10), 856–871.

Thiede, S., Ghafoorpoor, P., Sullivan, B. P., Bienia, S., Demes, M., & Dröder, K. (2022). Potentials and technical implications of tag based and ai enabled optical real-time location systems (RTLS) for manufacturing use cases. *CIRP Annals, 71*(1), 401–404.

Thiede, S., Juraschek, M., & Herrmann, C. (2016). Implementing cyber-physical production systems in learning factories. *Procedia CIRP, 54*, 7–12.

Thiede, S., Sullivan, B., Damgrave, R., & Lutters, E. (2021). Real-time locating systems (RTLS) in future factories: Technology review, morphology and application potentials. *Procedia CIRP, 104*, 671–676.

Touckia, J. K. (2023). Integrating the digital twin concept into the evaluation of reconfigurable manufacturing systems (RMS): Literature review and research trend. *The International Journal of Advanced Manufacturing Technology, 126*(3), 875–889.

Tran, T. A., Ruppert, T., & Abonyi, J. (2021). Indoor positioning systems can revolutionise digital lean. *Applied Sciences, 11*(11), 5291.

Tremblet, D., Yelles-Chaouche, A. R., Gurevsky, E., Brahimi, N., & Dolgui, A. (2023). Optimizing task reassignments for reconfigurable multi-model assembly lines with unknown order of product arrival. *Journal of Manufacturing Systems, 67*, 190–200.

Wang, G. X., Huang, S. H., Shang, X. W., Yan, Y., & Du, J. J. (2016). Formation of part family for reconfigurable manufacturing systems considering bypassing moves and idle machines. *Journal of Manufacturing Systems, 41*, 120–129.

Xing, B., Bright, G., Tlale, N. S., & Potgieter, J. (2006). *Reconfigurable manufacturing system for agile mass customization manufacturing*. Springer.

Yaoyuenyong, S., & Nanthavanij, S. (2008). Heuristic job rotation procedures for reducing daily exposure to occupational hazards. *International Journal of Occupational Safety and Ergonomics, 14*(2), 195–206.

Yi, G., Wang, Y., & Zhao, X. (2018). Evaluation and optimization of the design schemes of reconfigurable machine tools based on multiple-attribute decision-making. *Advances in Mechanical Engineering, 10*(12), 1687814018813054.

Zhang, M., Guo, H., Huo, B., Zhao, X., & Huang, J. (2019). Linking supply chain quality integration with mass customization and product modularity. *International Journal of Production Economics, 207*, 227–235.

Zheng, T., Ardolino, M., Bacchetti, A., & Perona, M. (2021). The applications of industry 4.0 technologies in manufacturing context: A systematic literature review. *International Journal of Production Research* 59(6):1922–1954.